1960

Web buckling tests on welded plate girders, Part 2: Tests on plate girders subjected to bending, WRC Bulletin, 64, (September 1960), Reprint No. 165 (60-5)

K. Basler

J. A. Mueller

B. Thurlimann

B. T. Yen

Welded Plate Girders, Report No. 251-12

Submitted to the
Welded Plate Girder Project Committee
for approval as a publication

WEB BUCKLING TESTS ON WELDED PLATE GIRDERS

Part 2: Tests on Plate Girders Subjected to Bending

by

Basler, K., Yen, B.T., Mueller, J.A., and Thürlimann, B.

Fritz Engineering Laboratory
Lehigh University
Bethlehem, Pennsylvania
May 1960

FOREWORD

This paper is the second part of a report on plate girder tests conducted at Lehigh University. Reference must be made to the first part, report No. 251-11, for the scheme of publication, the properties of the girders, the nomenclature, and the list of references.

2.1 Introduction

While the aim of the entire investigation is to evaluate the post-buckling strength of plate girders, it is the objective of this part to present the test results obtained from the girders subjected to pure bending.

The determination of a plate girder's strength beyond its web buckling load, the so-called post-buckling strength, first requires complete familiarity with the web buckling limit. Today, this problem can be considered to be almost solved, as the literature survey presented in part 1 indicates. Although the present investigation is not specifically directed toward any further theoretical studies of the web buckling load, attention will surely be focused on this phenomenon by these experiments. The more complex problem is the determination of the carrying capacity of plate girders. Even though a number of ultimate load tests on plate girders have recently been conducted, Ref. 137, 159, 161, 190, and 262, no strength predictions have yet been developed. The difficulty is that there are several parameters which influence a girder's strength. To keep the present investigation within reasonable and realistic limits, a restricted number of parameters were studied. These are

reviewed next.

The first parameter is the loading condition which may range from pure bending to high shear. A measure of this condition is the ratio of the shearing stress τ in the web to the extreme fiber stress σ of the flange, both evaluated at a representative cross section of the girder. Considered as a major factor in determining the strength of the bending girders, the shape of the compression flange is taken to be the second parameter. While this might appear unusual, it should be mentioned that the web buckling theory already allows up to a 60% increase in the critical load when the compression flange exhibits torsional rigidity. According to the buckling theory the most influential of all parameters is the web slenderness β, the ratio of the web's depth to its thickness. This has been amply investigated and is the third parameter entering the study. Finally the effect of the distance "a" between transverse stiffeners is considered as the fourth parameter and is expressed in terms of the web depth "b" as $\alpha = a/b$. The objective of the entire investigation can therefore be expressed as follows:

Problem	Parameter
	1. $\epsilon = \tau/\sigma = \frac{\text{shear stress}}{\text{normal stress}}$
Buckling Load of web influenced by:	2. shape of the compression flange
Ultimate Load of girder influenced by:	3. $\beta = b/t = \frac{\text{web depth}}{\text{web thickness}}$
	4. $\alpha = a/b = \frac{\text{panel length}}{\text{web depth}}$

If experimental evidence as to the influence of a parameter is to be obtained, more than a single test on a single girder must be conducted. For example, if a girder's ultimate load were twice as high as its web buckling load, to which parameter could this increase be attributed ? Therefore, at least two tests on girders which differ in no way except in the parameter under investigation are needed. Furthermore, the variation in this parameter should be extreme in order to achieve the most pronounced effect, since,then,the difference in results can not be ascribed to a random scatter. As will next be seen, the listed parameters and the use of this principle essentially determine the choice of the test girders' cross sections.

The first parameter was varied by dividing the entire test program into three groups: girders subjected to bending,

to high shear, and those under combined bending and shear. With this first parameter fixed for the bending girders, the investigation discussed in this report reduces to an evaluation of the influence of the remaining three parameters. This was accomplished by having five girders fabricated with the cross sections as given in Fig. 2.1. Girders G1, G2, and G3 appearing in the upper row were alike in every detail except in the shape of the compression flange. In the lower row of this figure the cross sections of girders G4 and G5 are given. These differed from the first series in web slenderness alone, thus allowing for a study of the third parameter β. Then, the final parameter was accounted for by choosing a transverse stiffener arrangement which subdivided each girder's test section into a long panel with $\alpha = 1.5$ and two short panels with $\alpha = 0.75$. If failure would occur in the longer panel, then, after reinforcing this damaged portion, failure might be expected to occur in a short panel. Consequently, a total of two ultimate load tests were anticipated for each girder.

2.2 Design of Girders and Test Setup

All five girders were tested in the setup which appears in Fig. 2.2. By using a constant cross section throughout a girders' length, failure would almost certainly occur in the neighborhood of the loading points where bending and shear stresses were both present at their maximum values. Therefore, end pieces designed with somewhat heavier webs to accommodate this condition were placed on both ends of the test section proper. By locating the splices nearly a girder's depth away from the loading points, the local influences of the concentrated loads were eliminated. With the test section bounded on either side by a stiffener which was again a foot away from these butt welds, the clearest possible loading conditions were achieved for the test section.

The size of the girders was essentially determined by the web thickness which should not be less than one eighth of an inch. Only under this condition could the regular shop fabrication methods be used which would cause residual stresses and welding distortions comparable to those existing in actual structures. Selecting the web depth to thickness ratio to be a maximum of 400, the resulting web

depth amounted to fifty inches which was consistently used for all the girders. With the available loading capacity of the jacks used in the test setup specified, the resulting length of the girders was about forty-five feet. While the overall dimensions appear in Fig. 2.2, reference should be made to Sec. 1.2 for the actually measured dimensions of the component plates.

The transverse stiffeners used are divided into two classes, bearing and intermediate stiffeners. Both types were symmetrically placed on both sides of the web and welded continuously to it. The bearing stiffeners, placed over the supports and under the loads, were of T-shapes cut from 12WF50 sections. They were milled on the bearing end and welded there to the girder flanges along the outside face of their own flange. All intermediate stiffeners were plates, 4"x $\frac{1}{4}$", welded to the web side of the compression flange. All the bearing and intermediate stiffeners were cut short of one flange: opposite the supporting points and along the tension flange, respectively.

The test setup was devised such that a simple determinate system resulted. Details at the supports are shown in the aforementioned Fig. 2.2 and a view of the overall

setup is given in Fig. 2.3. For further information on the loading frames, jacks, pendulum dynomometer, and test bed, reference can be made to Ref. 272. The loading device was calibrated with a Morehouse Proving Ring which complied with the requirements of the National Bureau of Standards. This calibration test showed that the dynamometer was well within standards required by the American Society of Testing Materials.

A final feature of the test setup was to guard against lateral instability of the girder. As seen in Fig. 2.4, $2\frac{1}{2}$" standard pipes were connected near the compression flange all along the girder and, in addition, near the tension flange at the loading points. These supports were pin connected to all transverse stiffeners as in detail A of Fig. 2.4. Through the use of one inch pins in the $1\frac{1}{16}$" holes at the ends of the pipes, a vertical deflection of five inches could be tolerated before the pipes would be strained. For deflections in excess of five inches, an adjustment in the elevation of the lateral braces was made.

2.3 Basic Test Observations

In conducting all the welded plate girder tests, certain observations were invarisably made. Three important ones are discussed next as expressed in a load-deflection diagram, a web deflection chart, and a plot of stresses measured by SR-4 gages.

Load-Deflection Curve

Instrumentation for this group of readings included scales mounted on the girder at various locations along its length and an engineer's level so positioned that all points along the girder could be brought into focus. The absolute girder deflections were obtained by computing the differences in scale readings between those at a specific load and the initial readings, which were the ones taken before the girder was loaded. Since the support movements were also observed by the level, the relative girder deflections were readily evaluated. In all the diagrams subsequently presented, it is this relative deflection which is plotted. With the engineer's level and the setup employed , observations of one hundredth of an inch were possible, which is well within the accuracy

demanded by the presented plots. A scale mounted on a nearby building column provided a stable reference and guarded against difficulties which might occur through level movements. Connected to the test bed, a dial gage provided a control on the testing speed and a check on the absolute centerline deflection.

Since the testing procedure was the same for all girders, a single specimen, girder G2, is selected as a typical example for discussion. Before testing, characteristic loads were computed for the girder in order that a loading increment could be decided upon. Having yield and plastic loads of P_y = 149 and P_p = 167 kips per loading jack respectively (Table 1.7), increments of 18 kips were selected. After each load increment was applied, a set of readings was taken and a number assigned to this "load station" to define the sequence of load applications. With this loading pattern, enough observations were available for study without causing undue delay.

Plotted in Fig. 2.5, is the applied jack load P versus the centerline deflection. The ordinate,being the load, is given in kips and the abscissa is the deflection in inches. A second ordinate listing the corresponding extreme fiber

stress of the top flange in kips per square inch, enables a judgement of the magnitude of the load with respect to the more conventional stress criterion. Also given are the critical load P_{cr}, the yield load P_y, and the plastic load P_p as well as the predicted elastic centerline deflection v_{ℓ}, Sec. 1.7.

At zero load, load No. 1, a complete set of readings was taken and then the load was gradually increased up to 18 kips, termed load No. 2, where another set of data was recorded. Following this procedure, the load was increased to a point where inelastic behavior was noticed, load No. 8 at 126 kips. This was indicated by the deviation of the load-deflection curve from a straight line as well as the appearance of some yield lines on the girder. At this load, which was estimated to be close to the ultimate load, another full set of measurements was taken and then the girder was completely unloaded, load No. 9.

Between loads No. 9 and 10, the girder was loaded up to 126 kips ten times to give evidence that a limited number of repeated loads would cause no additional distortions in the girder. As shown in the load-deflection diagram as well as in the other plots, additional distortions were non-

existant and all the girders performed elastically within this load range. Beginning with load No. 10, zero kips, the load was increased up to load No. 19, 126 kips. The next deflection data was recorded at load No. 23, at 135 kips. Then a very low strain rate was imposed on the girder and the deflection at each kip was recorded by means of the centerline dial. After reaching a dynamic ultimate load of 140.2 kips the load began to drop. At this point the applied strain was held constant and the load stabilized at 135 kips, load No. 24. The load of 135 kips was considered to be the static ultimate load P_u. With all data recorded at this load, the girder was unloaded and the first test, T1, was completed with load No. 25.

Failure in this first test was due to lateral buckling of the compression flange, occurring over the longer panel of the girder where the spacing of the lateral braces was greatest. By reinforcing this portion of the flange, failure could be forced into another panel, thus producing a second, independent test. This was done by welding two steel plates along the failed portion of the flange, one on each side. Due to the welding, a slight increase in the girder deflection occurred, as shown between load No. 25

and 28.

With the reinforcement added, a second test was begun and again load increments of 18 kips applied. The highest static load reached was load No. 37, 144 kips. Again by employing a low strain rate, a somewhat higher dynamic maximum load of 144.6 kips was observed after which the load decreased to load No. 38 at 142.6 kips. In this second test, T2, the ultimate load was considered to be 144 kips. Since the girder was no longer useful after that, an unloading curve was obtained by increasing strains and observing the load at which the deflection could be held constant. After obtaining a total centerline deflection of about six inches at load No. 51, 81 kips, the girder was unloaded to zero kips, load No. 53, and the testing of G2-T2 was at an end.

Thus, the complete loading history of any single girder is obtained from its load-deflection diagram. With the extensive explanation presented above, the loading histories of the other four girders can be similarly obtained from their load-deflection curves. For these, reference must be made to Figs. 2.6, 2.7, 2.8 and 2.9 appearing at the end of this report.

Web Deflections

The purpose of this graph is to present pictorially the deflection of the web out of its plane for a number of loads and locations. Because the graphs for all the girders are similar, a single one can be described and the explanation will be sufficient for understanding all others. As done for the load-deflection curve, the representative web deflection graph is selected to be that of girder G2. In order to locate the points at which reading were taken, extensive use of a Cartesian coordinate system was made whose origin and orientation is defined in Fig. 2.10. As seen, the XY plane coincides with the central plane of the web. The X-axis extends along the mid-depth of the web and the Y-axis, positive upward, coincides with the vertical centerline of the girder. Referring to the photograph of the test setup in Fig. 2.3, the Z-axis is positive in the direction opposite to the lateral bracing pipes while the X-axis points to the right. With this system, the locations of the web points at which measurements were taken are as given in Fig. 2.10. Incidentally, this figure also shows the scales used in measuring girder deflections, the location of all SR-4 strain gages, and the position of all fixed dial gages.

A special dial rig was made to measure the desired web deflections. This rig was composed of a portable steel frame and deflection dial gages: horizontally mounted gages to obtain lateral web deflections, and vertically mounted gages to record the relative movements of the flanges. An overall view of this dial rig while in a measuring position is shown in Fig. 2.11. The rig touched three points of the girder: the bottom flange at a point half an inch away from the web surface, the web at a point just above the fillet weld along the bottom flange, and again the web just below the top flange, held there by a strong magnet. Being extremely mobile and easy to read, the rig could readily be moved to differend cross sections and thus accounted for more than 20,000 readings during the course of this investigation. All dial gages were AMES dials with a least dial division of one thousandth of an inch and a stem stroke of one inch. When a dial ran out of stroke, specially machined steel blocks of known thicknesses were used to bridge the gap.

In order to obtain the initial distortions of the girder, a special calibration block was fabricated such that, when the dial rig was inserted in it, the web dials

measured a perfect plane surface. At the same time the flange dials recorded fictitious flanges which were fifty inches apart and perpendicular to the web plane. The reference readings obtained could always be reproduced within one thousandth of an inch when repeatedly put in this carefully milled block. However, after a girder was whitewashed and this procedure tried on the girder, a scatter within $\pm$ 0.004 inches was unavoidable.

Having defined the stations at which the web deflections were observed and having described the dial rig used to obtain them, an explanation of their graphical reprentation is in order. In the upper portion of Fig. 2.12 the girder's test section is outlined with its stiffeners, indicated at X = - 75, - $37\frac{1}{2}$, 0, and + 75, subdividing the section into three panels. The coordinate system, explained before, is shown at the center of the section. The measured data, indicated by the dots and plotted along a vertical line representing the cross sectional location, appears in the plane of a cross section which has been rotated clockwise 90° about the vertical line. Thus, web displacements w, extending in the Z direction, are negative if they are plotted to the left of the cross sectional line, positive

if to the right. By plotting the web deflection, w, to a scale 12 times that in which the girder is shown and connecting the dots by straight lines, the distorted cross sections can be visualized. For consistency, the flange distortions are also shown in this scale.

Deformations are shown for three different loads: load No. 1, P = 0 kips, in order to obtain initial web distortions; load No. 5, P = 72 kips, to obtain deflections at about the critical load P_{cr}; and finally at load No. 8, P = 126 kips, to obtain web deflection at about ninety percent of the ultimate load P_u. The following can be seen from this plot:

- All initial distortions were on the same side of the girder.
- The largest initial web deflection recorded in the test section was 0.170 inches at X = + $37\frac{1}{2}$, Y = 0.
- Additional web deflections up to about ninety percent of ultimate load were of the same order of magnitude as the initial ones.
- The greatest web deflection recorded up to load No. 8 was 0.306 inches at X = + 50, Y = + 9.

- As the load increased, the single wave pattern along X-direction in the longer panel gradually changed into a double wave pattern.
- Relative movements of the flanges were so small that, within the accuracy of the drawing, they coincided with the initial distortions for the loads recorded here.
- The shape of the cross section was so carefully observed that even the kink in the flanges, caused by the fillet welds, appears.
- Finally, the initial deviations of the transverse stiffeners from a perfect plane were measured. Remaining rigid throughout the tests, they incurred no added deflections.

While the diagram in the upper portion of Fig. 2.12 contains all points at which deflection readings were taken, it only presents three load stations. Supplementing it, therefore, are the three diagrams in the lower half which give all the load stations at which readings were observed for three representative points in the web, one from each panel of the test section. Thus, the upper portion essentially depicts the shape of the deformed cross sections while the rate of growth of the deflection is indicated in

the lower part. The characteristics of these curves are essentially the same as those of the load-deflection curves for the girder. Deflections gradually increased with load, almost completely recovered after unloading, acquired no cumulative increase after the girder was subjected to the repeated loading, and had finite values at the end of T1. Of major significance, at the computed web buckling load of 74 kips, the web deflections increased as gradually as before with no sudden changes appearing.

Again, with the help of the above explanation, the corresponding diagrams of the other four girders appearing as Figs. 2.13, 2.14, 2.15, and 2.16 can be interpreted. More convincing than words, these figures clearly show that a web buckling load can not be observed on shop fabricated, welded plate girders.

Bending Stress Distribution

The last basic observation to be discussed here, the measurement of girder bending strains, provides a check on the bending stresses which, according to beam theory, are computed as $\sigma = \frac{M}{I} y$. To determine these stresses or strains, SR-4(A1) electrical resistance strain gages were mounted at

various points throughout a cross section as previously indicated in Fig. 2.10 for G2. In this arrangement, typical for all bending girders, gages were located at two cross sections, X = - 18 and X = + 40, both near the center of their respective panels. In all cases, gages were placed in pairs, one on either side of the web. Thus, bending strains and membrane strains could be differentiated.

As done before, girder G2 is selected as the representative girder whose results are to be discussed. In Fig. 2.17 are shown the data observed from this girder. To the left are plotted the strains for the cross section at X = - 18 and to the right those for X = + 40. Below the stress and strain scales in the upper portion, the outline of the girder and the strains predicated by the ordinary bending theory are shown in thin lines. The dots indicate measured values and those corresponding to the same load are connected by the heavier lines. It can be seen that at high loads the portion of the web in compression carried less stress than would be assigned to it by the beam theory. By deflecting laterally, as illustrated in the previous discussion on web deflections, the web reduced its membrane stresses, while transverse plate bending stresses were

created. This becomes evident by studying the load-strain diagram for a particular web point as shown in the lower left-hand portion of the plots for each cross section.

The particular point on the web chosen at each cross section under investigation is at Y = + 15. An inclined thin straight line labelled "th" in a diagram gives the prediction of the beam theory and the dots represent the observed test data on both sides of the web, $Z = -\frac{1}{8}$ and $Z = +\frac{1}{8}$. The curve Z = 0 was obtained by averaging two corresponding strain readings. If the web would remain plane, these strains should be the same and would increase linearly along the predicted line. From the web deflection drawing, Fig. 2.12, it is seen that the web deflected such that the plate bending stresses were tensile on the far side of the web, $Z = -\frac{1}{8}$, and compressive on the near side. By superimposing these stresses onto the compressive membrane stresses, the surface stresses on the far side must increase at a smaller rate than those at the near side. This is indeed borne out by the diagram. Certainly, no sudden bifurcation of the surface stresses at the predicted web buckling load could be observed.

Finally, in the lower right-hand part of the plot for

each cross section, the strains as observed at the extreme fibers of the top and bottom flanges, Y = + $25\frac{3}{4}$ and Y = - $25\frac{3}{4}$ respectively, are compared with the predicted values labelled "th".

The explanation of the above diagrams applies to all the other plots of the remaining girders. These figures, appearing at the end of the report, are Figs. 2.18, 2.19, 2.20 and 2.21.

With the load-deflection curves presented for each girder and the other two basic measurements expressed in graphs, a discussion of the ultimate loads and failure modes follows.

2.4 Ultimate Loads

In this section reference will be made to such characteristic loads of the girders as their critical load, P_{cr}, yield load, P_y, and plastic load, P_p. The definitions and details of computation of these loads have been consolidated in the first report and the resulting reference values are here again summarized in Table 2.1.

Whereas P_{cr}, P_y, and P_p are loads computed from girder properties, the ultimate load is an experimentally obtained value. It is defined as "the highest observed jack load which could be maintained on a girder and hence was obtained at zero straining rate". This definition is necessary in order that values on the conservative side result. For, as was pointed out in Sec. 1.3, the yield level of mild steel is considerably affected by the speed at which it is tested. Thus, in order to eliminate this effect, the static yield level must be considered as the significant datum. The method used to arrive at this yield level during the girder tests is explained next.

Referring to the load-deflection curve of girder G2, Fig. 2.5, it is seen that the last load station reached

before failure occurred in the first test was Load No. 23 at 135 kips. After maintaining this jack load of 135 kips for a few minutes, the centerline deflection dial stopped travelling and a complete set of observations was made over a period of forty minutes. Thus, disregarding extended time effects such as creep, a zero straining rate was surely obtained and the girder could certainly maintain this load. Thereafter, the girder was loaded slowly with the aim of increasing the load by another increment of nine kips. After the girder was loaded to a maximum of 140 kips, the deflection increased without any corresponding increase in load. At this point, the deflections were stabilized and, after a few minutes, the load settled at 135 kips, load No. 24, where another set of readings were taken. If load No. 24, following the maximum or ultimate dynamic load, would have been greater than load No. 23, then it would be considered as the ultimate load, since it also could be held at zero straining rate. As seen for girder G2, the ultimate static and dynamic loads were 135 kips and 140 kips, respectively. A summary of all static and dynamic ultimate loads is given in Table 2.1, where P_u and P_{max} are used as their respective designations.

The procedure outlined above was followed for every girder tested. Admittedly, the determination of the highest load which could be statically maintained depended somewhat on the judgement of the investigators. Using smaller load increments in the vicinity of the ultimate load, this test, G2-T1, might have yielded a static ultimate load of 137 kips. However, the ultimate loads P_u decided upon are certainly conservative and, at best, could have been only a bit higher.

As a matter of record, the time element during testing is included now. Each single test took about one full day. By reinforcing at night, the second test could be run the second day. A load increment of 18 kips was applied in about five minutes on the average, producing a centerline deflection rate of about 0.08inches per minute. Near the ultimate load, this rate was dropped to about 0.01 to 0.03 inches per minute. At each load station designated with a number and marked with a circle in the load-deflection curve, the load was maintained for thirty minutes or more.

A comparison between the static ultimate loads of all the bending girders is done with bar graphs. In order to avoid misinterpretations, three plots are included,

Figs. 2.22, 2.23, and 2.24, each with a different reference. In Fig. 2.22, where the yield load is the non-dimensionalizing factor, it appears as if the girders with the tubular compression flanges, girders G3 and G5, would be distinctly superior to those with conventional flange plates, girders G2 and G4. But these girders with the tubular top flanges have their extreme flange fibers considerably farther away from the neutral axis than do the conventional shapes of the same web depth. Since the flange centroids essentially determine the lever arm of the flange forces, a more realistic comparison of strength is obtained when the plastic load is used as a reference. This is done in Fig. 2.23 where it is seen that the difference between the two shapes almost completely disappears.

A third graph is drawn with the ultimate strength measured in terms of the amount of steel needed to build the test section. This graph is given in Fig. 2.24. The denominator for the ordinate is the product of the cross sectional area A and the compression flange yield stress σ_{yf}. The area is directly proportional to the weight and the significant yield stress is needed such that a fair comparison can be drawn between girders with different yield

levels. From this graph it is seen that bending girders become more and more economical as the web slenderness ratios increase. For a given depth, cross sectional area, and yield stress, this conclusion can readily be visulized. For, as more material is distributed to the flanges, the lever arm within the cross section increases and so does the bending moment. Obviously, there must be a limit because the web will eventually become so weak that it cannot brace the compression flange properly. Confirmation of this action was obtained in the second test of girder G4. A discussion of this failure and the failure modes of all the girders will, therefore, have to be added to the ultimate load data. This is done in the next section.

2.5 Failure Modes

Here, the special features of each girder's failure will be discussed together with observations concerning the girders.

Girder G1

The conventionally used buckling theory predicts, for this girder, the occurence of web buckling at P = 70 kips and flange buckling at P = 73 kips, where P is the applied load of one jack. These buckling loads are well within the elastic range since P_y, the load which initiates yielding in the flange's extreme fiber, was computed to be P_y = 131 kips. Of prime interest is the answer to the question of how the girder fails. Will it carry the bending moment in pure beam action up to about P = 70 kips and snap into a wavelike buckling pattern ? Will the top flange buckle shortly thereafter ?

The girder was loaded in increments of nine kips up to P = 54 kips, load No. 7, as seen from Fig. 2.6. At this point, failure seemed imminent, since the top flange distortions were anywhere from one to two times the flange

thickness. But when unloaded to load No. 8, P = 0 kips, these distortions almost completely recovered. An appreciation of the growth and disapperance of the flange deflections may be gained from the two photographs in Fig. 2.25 which were taken along the compression flange at loads No. 7 and 8 respectively. In the second loading cycle from zero to the ultimate load of 81 kips, loads No. 8 to 14, these distortions appeared once again. They reached very high magnitudes by the time the ultimate load was finally obtained between loads No. 14 and 15. An overall view of the girder at load No. 15 is given in Fig. 2.26 where the alternating inclination of the compression flange from one panel to the next appears clearly.

The twisting of this flange gave rise to an interesting yield line pattern on its surface. Local plate bending stresses, alternately tensile or compressive depending on whether the plate was convex or concave, were superimposed on the flange compressive stresses and eventually led to yielding on the flange's surface. At the welds, the residual stresses are always tensile, hence no yield lines were found along the fillet welds joining the compression flange to the web.

Unquestionably, the impression left from this first ultimate load test was that the web and flange deflections increased gradually and, even in the vicinity of the ultimate load, no sudden changes in their rates of growth were observed. This is borne out by the web deflection chart, Fig. 2.13. In the lower left corner of this figure a typical cross section at $X = -12\frac{1}{2}$ inches was drawn with its web deflections and flange distortions as they appeared for loads No. 8 to 14. In the lower right corner, the rates of deflection are expressed by plotting some non-dimensionalized web deflections against applied loads. These plots bring out the fact that the rates of deflection were about the same for all points in a cross section, that is, the predetermined deflection mode did not change throughout the test.

The ratio of the width of the outstanding flange leg to the flange thickness was $c/d = 24$ in the first test. It was hoped that, after this test, the flange width could be reduced and all residual distortions eliminated by cold straightening thus a second independent test might be conducted on a new cross section with a c/d ratio equal to 16. But during the course of cold straightening, upon releasing

the applied restraints, the flange snapped back into its original wave pattern with distortions in the order of its thickness. Having only reduced the width of the compression flange to 13.6 inches but not completely removed the distortions created during the previous test, the girder was retested. Even with these large deformations, a flange stress of 26 ksi was obtained as compared with 22 ksi observed in the previous test. For the values of these stresses, reference can be made to the two stress ordinates in Fig. 2.6 which give the extreme fiber stresses corresponding to the applied loads for both tests. It must be kept in mind that this second test can not be expected to verify any theory, and references to it should not be made without including an explanation of its unfavorable initial condition.

Girder G2

Proportioned generally according to regular design practice, this girder's web slenderness ratio of $\beta = 185$ was greater than the specified limit of 170. The only difference between girders G1 and G2 was that the ratio of the compression flange's outstanding width to thickness

was c/d = 8 for G2. This ratio, according to Ref. 269, should have insured that a torsional flange failure would not occur before the flange reached the strain hardening condition.

The girder was loaded beyond the computed critical load of P_{cr} = 74 kips with no sudden web buckling observed, and the ultimate load was reached at P = 135 kips, 91% of the computed yield load. Failure occurred on the compression flange over the longer panel by lateral buckling which was measured using the following setup. Clamps were secured to the upper ends of the bearing stiffeners at both supports and a wire stretched taut between them. Considering the rigidity of these stiffeners and their rigid connection to the supports, the wire was assumed to be an absolute reference for lateral flange movements. Distances between this wire and predetermined points on the flange were made with a scale.

The results of these measurements are presented in Fig. 2.27, where the data is plotted for two zero loads, No. 21 and 25. Measured before the girder was loaded to its first ultimate load, the results for load No. 21 show the variation of the initial flange shape from a straight

line. After failure, measurements of load No. 25 were made. The change in shape between these two measurements is the buckling shape. Although lateral braces were provided at every intermediate stiffener, the observed buckling length was somewhat more than the greatest unsupported length. This discrepancy is partially explained by the fact that small movements of the lateral supporting pipes were possible since the connecting pins and holes used were 1" and $1\frac{1}{16}$" in diameter respectively. In addition, the beam to which the bracing pipes were connected was not absolutely rigid, permitting some small elastic movement under a heavy bracing force. As a reasonable value for the buckling length, l_k, a value of 100 inches was selected for the first test and 50 inches for the second test. The choice of this second value will become clear when the reinforcement added to the girder prior to the second test is discussed. Since lateral buckling of the compression flange occured always in the inelastic buckling range, slight variations in the estimated buckling length have little effect on the computed lateral buckling load.

At load No. 6, about 0.6 P_y, the first yield lines appeared on the girder, indicating the presence of residual

stresses caused by welding. Characteristically, they were initiated at the tips of the compression flange where residual compressive stresses exist, Fig. 2.28. By adding the compressive stresses due to the applied bending moment to these residuals, the yield limit is reached earlier than predicted by P_y. This effect is always intensified at locations where transverse stiffeners are welded to the flange, as also seen in Fig. 2.28 which gives a typical yield line pattern in a compression flange. On the outside surface of the tension flange, yielding would be expected to occur first at the intersection of the flange and web. Indeed, this was the case, but, contrary to predictions, the tension yield lines always appeared at loads higher than those causing first yielding in the compression flange. This may be explained by the fact that yield lines occur when slip bands, which have formed in the material, have spread or flowed to such an extent that the brittle mill scale and whitewash on the surface will pop off the steel. Since the area over which high residual tensile stresses occur is comparatively small, the slip band will not spread over a wide region of the flange plate and the scale will not flake off the surface. Furthermore, the mill scale and whitewash may behave differently in

tension than in compression and may fracture in tension without immediately falling off the steel surface.

The presence of residual stresses was also indicated in the load-centerline deflection curves. From Fig. 2.5 it is clearly seen that the "proportional limit" is exceeded beyond load No. 6, whereas the stress-strain diagrams obtained from the tension coupons, Fig. 1.7 in Sec. 1.3, reveal no such deviation from a straight line prior to yielding. The reason this did not occur in the coupons is that by being cut out of the plates, they were essentially free of all residual stresses introduced during the rolling and welding operations. The second loading path of Fig. 2.5, loads No. 10 to 19, followed a perfect straight line because the residual stresses were removed during the first loading cycle to such an extent that every fiber behaved elastically within this range.

Before the second test of girder G2, the buckled flange was reinforced by welding a 4" x $\frac{1}{4}$" plate along both edges of the top flange. A sufficient increase in lateral rigidity was imparted to the buckled length that further lateral deflections could not cause failure in this long panel. Therefore, in the second test which began with load No. 28

and ended with load No. 53, attention was focused on the two short panels. With a spacing of the lateral braces half that of the first test, a different type of failure was anticipated. After pronounced yielding, local torsional buckling occurred as appearing in Fig. 2.29.

Girder G3

Differing from the two previous girders in the shape of the compression flange alone, the mode of failure of this girder was restricted to one type. Unlike the wide flanged girder G1 which buckled torsionally and the compact flange of girder G2 which buckled laterally in the first test and twisted in the second, the tubular flange demanded a lateral buckling failure.

This was indeed the case in the first test of this girder G3-T1. The observed lateral deflection of the compression flange appears in Fig. 2.30 where the load stations for this diagram are 1, 19 and 21. The subsequent reinforcement added after the first test is similar to the one for girder G2, that is, a pair of steel plates was added to the failed portion of the flange (Fig. 2.31). In the second test failure was again due to buckling of the com-

pression flange in the lateral direction. A photograph of this girder's test section, taken after both tests were completed, is given in Fig. 2.31.

In all tests, the lateral bracing forces were recorded by mounting SR-4 gages on both sides of the bracing pipe located at X = 0. The results obtained for girder G3 are plotted in Fig. 2.32, where the ordinate is the applied jack load P and the abscissa is the measured axial load in the pipe. From this figure, and from similar ones for other girders, it is seen that bracing forces were non-existent until yielding of the flanges become apparent. Thereafter, the forces depended greatly on the extent of straining which the compression flange underwent after the ultimate load was reached. According to the linear buckling concept, braces need only be designed with a certain rigidity. However, when initial girder "imperfections" are present and inelastic instability occurs, it is likely that considerable bracing forces must be provided if the girder strength is not to be impaired by insufficient lateral bracing. In the second test of girder G3, these forces were of such a magnitude that a bearing failure under the pin in the transverse stiffener occured. It

could well be that a more rigid bracing system with no play in the pins would have reduced the magnitude of the lateral deflections and thus reduced the required bracing force.

Girder G4

Girders G1, G2, and G3 differed in the shape of the compression flange, with lateral and torsional buckling of the flange constituting their failure modes. As far as the flanges are concerned, girder G4 was a duplicate of girder G2, but it had a web slenderness ratio of 388, about twice as high as that for G2. This resulted in a computed web buckling load of about one quarter of that of G2, with P_{cr} = 15 kips and P_y = 130 kips.

As recorded in the load-deflection curve Fig. 2.8, the girder was loaded in small increments of nine kips of jack load. Up to a value of P = 108 kips, the girder's performance did not differ from that observed for girder G2. Some yield lines formed in the compression flange, first recorded at P = 75 kips. The flange, as it appeared at load No. 13, P = 108 kips, is illustrated in Fig. 2.28 which is also typical for girder G2, and therefore, is interpreted in the section for G2. Upon reloading the

girder ten times up to 108 kips and observing no changes in the web and centerline deflections, the load was increased beyond 108 kips and finally maintained at P = 118 kips, load No. 22. When an attempt was made to increase the load by another nine kips, pronounced yielding set in and, accompanied by a loud noise, failure occurred by lateral buckling of the top flange as was the case for the first test of girder G2. In place of a lateral deflection diagram, Fig. 2.33 provides a photograph of the top flange taken at load No. 23, just after the ultimate load was reached. It shows quite clearly the compression flange buckle with its peak at the center of the long panel. A close-up picture of the flange at this peak, Fig. 2.34, shows that the density of the yield lines increased on the concave side of the flange, having the appearance of a yield hinge. The failure of this girder was discussed in Ref. 7, p. 30, where it become apparant that the formation of a double waved web deflection pattern caused this type of failure and was responsible for the suddenness, noise, and impact.

By using the same reinforcement for this specimen as for girder G2, a second, independent test T2 was conducted. After P = 125 kips, inelastic behavior was noticed as can

be seen in the load-deflection curve. After a readjustment of the loading jacks, unloading and further reloading of the girder took place. Thereafter, yielding occurred once more in the compression flange of the test section's two smaller panels. When a yield line concentration appeared in this flange over the panel from X = - 75 to X = - $37\frac{1}{2}$, an attempt was made to stop the straining, but all in vain. With a tremendous noise and in an explosive manner, the compression flange pushed into the web of this panel. Figs. 2.35 and 2.36 illustrate this failure mode.

Girder G5

The testing history of this girder is recorded in its load-deflection curve, Fig. 2.9. As in girder G3, failure occurred by lateral buckling of the compression flange in both tests, although its web slenderness ratio of 388 was about double that of girder G3. A photograph of the top of the compression flange appears in Fig. 2.37, showing its configuration after both tests were completed. In the next picture, Fig. 2.38, an elevation of the test section is given which shows the deformations of the two short panels. It is clearly seen how the thin web distorted or

folded in order to be compatible with the buckled compression flange. Taking any one cross section through this folded web, there would be points of very high curvature along its depth. The web deflection pattern is, therefore, quite different from any wave pattern that could be predicted by the theory of elasticity.

When comparing the ultimate loads of girders G4 and G5, little difference exists. However, not all the characteristics of the girders can adequately be expressed by numerical values of strength. One item, whose importance is generally overlooked because it does nót affect conventional designs, is the ultimate flange strain that can be sustained prior to the ultimate load. For instance, if a section of a statically indeterminate plate girder were able to sustain a curvature well beyond that which produces first yielding, it is possible that a redistribution of moments might take place. Should the failure occur suddenly with no "rotation capacity" beyond the elastic limit, a redistribution of moments would not only be impossible but residual moments due to erection or support settlements might help to initiate the failure even earlier than expected.

Since all five girders were tested in the same setup, the obtained centerline deflection can be used to compare each girder's ability to deform while still maintaining load. Thus, the recorded load-deflection curves of the second tests of girders G2 to G5, together with G1-T1, are superimposed in Fig. 2.39. The difference between girders G4 and G5 is clearly seen here. Even in statically determinate girders, behaviour like that of girder G5 would give ample warning of an imminent failure while still increasing load. But cases similar to that of girder G4 would be more dangerous, since sudden collapse would be unavoidable.

2.6 Discussion

The objective of the investigation was to verify the predicted web buckling loads, to determine the post-buckling strength, and thus to form an opinion on the required factor of safety against this instability type of failure.

Web buckling, as predicted by the conventionally used theory of elastic stability, should manifest itself in a sudden lateral bulging of the web. As pointed out in the discussion on the web deflections, Sec. 2.3, no such phenomenon could be observed. The webs did deform, but in a gradual manner and, generally, this deformation amounted to an increase of the distortions put into the web during the process of fabrication. The buckling modes, as derived by the linear theory, would be such that the following numbers of half waves in longitudinal direction should appear:

	pin ended ($k = 23.9$)	fixed ended ($k = 39.6$)
short panel, $x = 0.75$	1	2
long panel, $x = 1.50$	2	3

As seen from an inspection of Figs. 2.12 through 2.16, the

number of half waves per panel differs and, with the exception of girder G1, they were not even alternating half waves but complete waves pointing to the same side of the web. This is due to the welding sequence. Welding the stiffeners first on one side introduces web deflections toward this side of the web. Turning the girder and completing the welding from the other side may reduce the magnitude of the previously introduced deflections somewhat, but leaves a deflection pattern which is consistently unsymmetrical to the true plane of the web.

Girder G1 was so designed that the critical stress of the compression flange plate exceeds that of the web only slightly. Hence, the compression flange offers little restraint to the web and since all the panels become critical at the same load, practically no restraint can be obtained at the loaded edges of the web plate. Therefore, the assumptions of the conventionally used buckling theory are fairly well fulfilled. But the carrying capacity, as seen from Table 2.1, is only 15% higher than the predictions of the web buckling theory. Thus the post-buckling strength of this girder is only 15% of its computed web buckling load. On the other hand, girder G4 exhibits an ultimate

load which is about 800% above the computed web buckling load. Admittedly, the actual boundary conditions for the panels of this girder differed from the assumptions of simple support, being closer to full restraint along the flanges. This would increase the buckling coefficient k from 23.9 to 39.6, that is about 60%; therefore the restraining influence of the compression flange can not be advanced as the explanation for the discrepancy between predicted web buckling load and actual ultimate load.

In Fig. 2.40 the ratio of critical stress to yield stress, σ_{cr}/σ_y, is plotted versus the web slenderness ratio β. Furthermore, the actually obtained stress ratios, σ_u/σ_y, are also given, σ_u being the ultimate web stress, computed as $\sigma_u = \frac{M_u}{I} Y$, with Y = 25 inches, $M_u = P_u \cdot 150''$ (Fig. 1.1), and I the moment of inertia of each girder (Table 1.6). The plot is slightly inconsistent as the yield stress needed to non-dimensionalize the critical stress has to be a constant value while the one for the girders varies somewhat. But, anyway, with this reservation the obtained post-buckling strength can be visualized from Fig. 2.40. It is seen that there exists no consistent ratio between the ultimate web stresses and the computed critical one. There is no possibility of expressing the ultimate stress as a multiple of

the critical stress, say 50% beyond σ_{cr} (the thin curve in the figure). The conclusion is that the web buckling theory will not predict the carrying capacity of thin web plate girders subjected to bending.

It was demonstrated that web buckling can not be observed as a sudden phenomenon. It is now seen that the theoretical predicted buckling loads have no bearing on the girder's strength. Why, then, should a plate girder be designed against something which does not determine the strength nor affect the appearance ? The conclusion from these tests is that the problem statement is inadequate; there is no justification in trying to formulate the post-buckling strength based on the buckling value. What is important is the ultimate load, upon which the design should be based.

These tests did not only lead to this conclusion but at the same time also gave an idea of what caused failure. First of all, in all ten conducted tests girder failure was due to a failure of the compression flange. Secondly, in nine out of ten cases failure was due to lateral buckling or torsional buckling of this flange. These observed failure modes, with the exception of the second

test in girder G4, were failure types which would have determined the carrying capacity of the girder whether it possessed a thin or a thick web. It will now be the task of the theoretical paper, which parallels this test report on girders subjected to bending, to formulate the ultimate moment a girder can carry in terms of the compression flange properties.

Table 2.1

Summary of Reference and Experimental Loads

Girder	Test No.	Theoretical			Experimental	
		P_{cr} (kips)	P_y (kips)	P_p (kips)	P_u (kips)	P_{max} (kips)
G1	T1	70.1	131	148	81	85.4
	T2	41.9	101	118	72	76.0
G2	T1	74.1	149	167	135	140.2
	T2				144	144.6
G3	T1	82.1	116	156	130	132.0
	T2				136	141.5
G4	T1	15.3	130	139	118	126.8
	T2				125	128.0
G5	T1	17.0	105	134	110	114.5
	T2				124	127.0

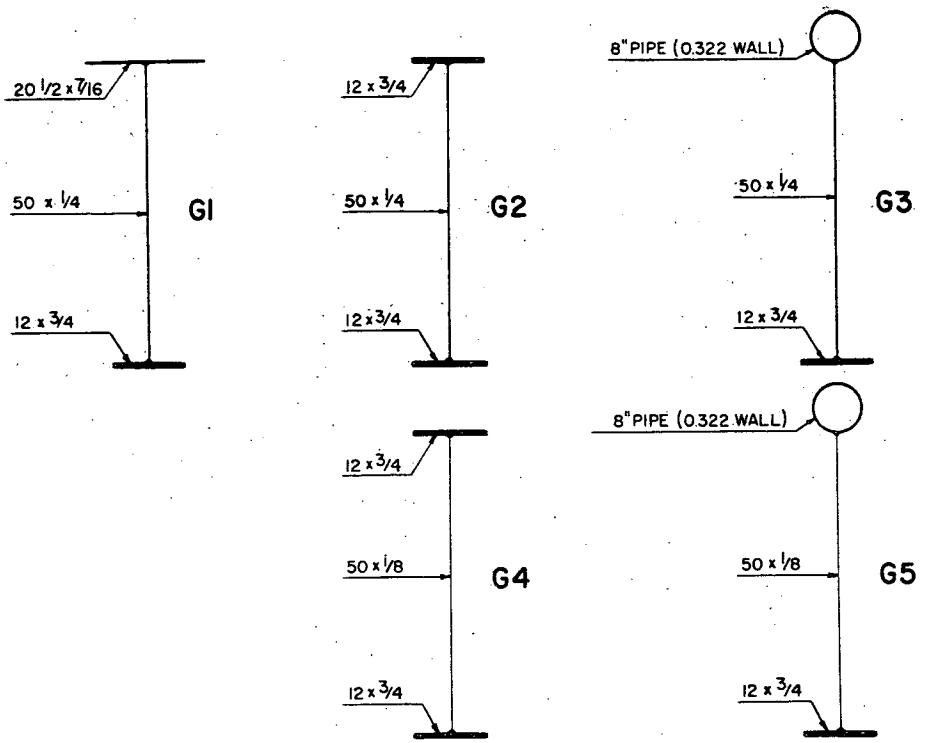

Fig. 2.1 - CROSS SECTION OF GIRDERS G1 TO G5

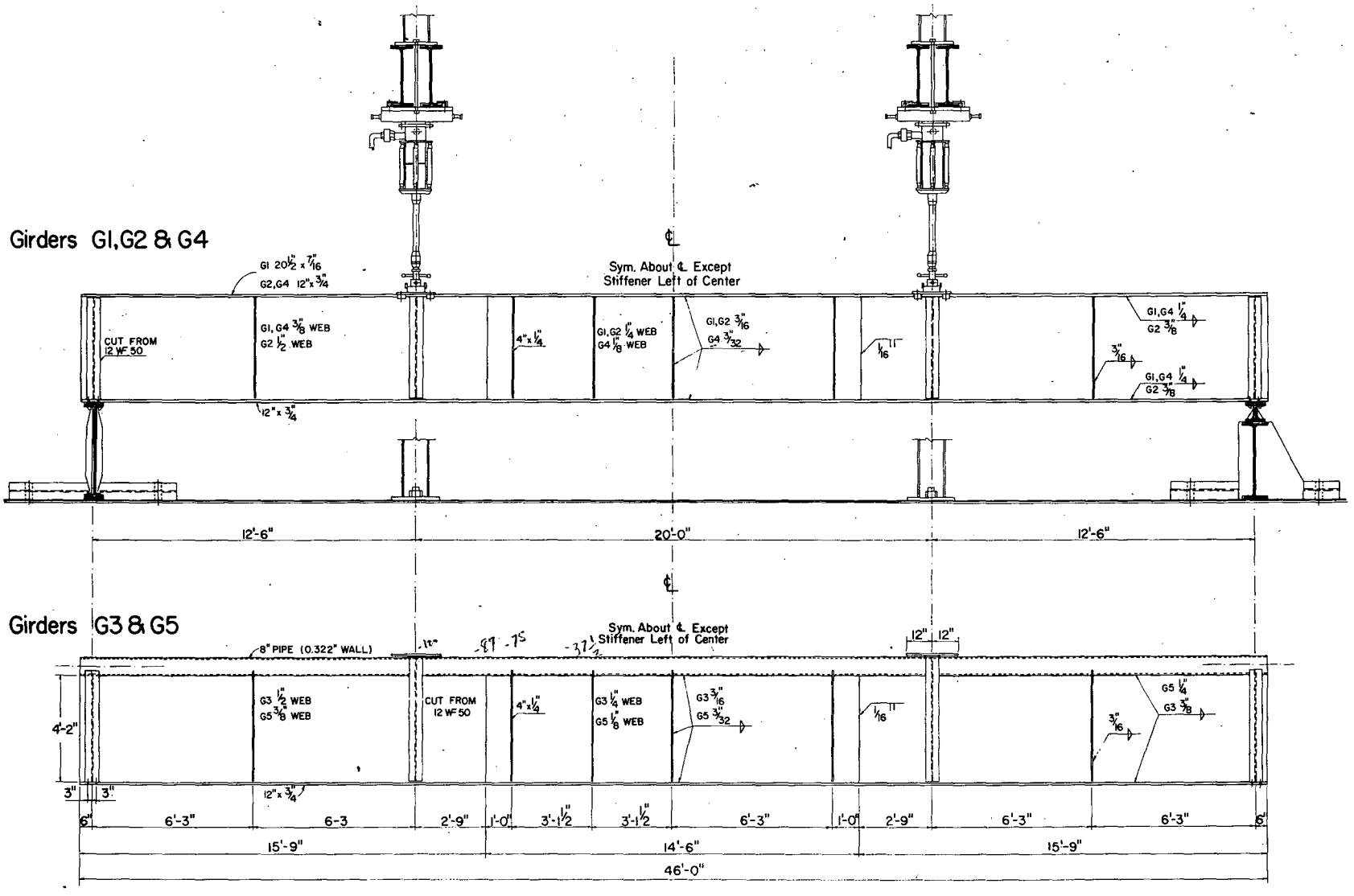

Fig. 2.2 Plate Girders G1,G2,G3,G4 & G5 with Test Setup

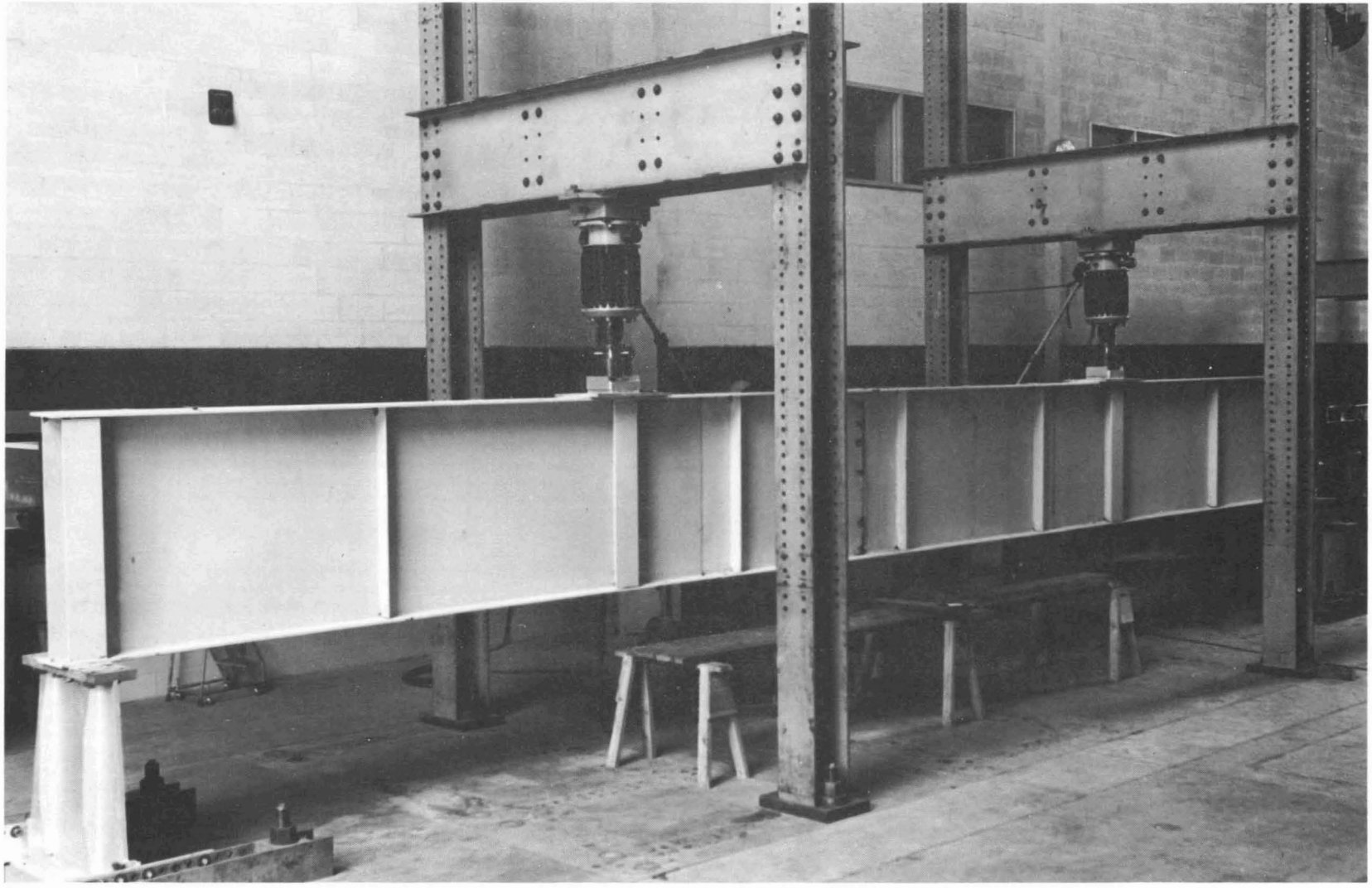

Fig. 2.3 Overall View of Test Setup

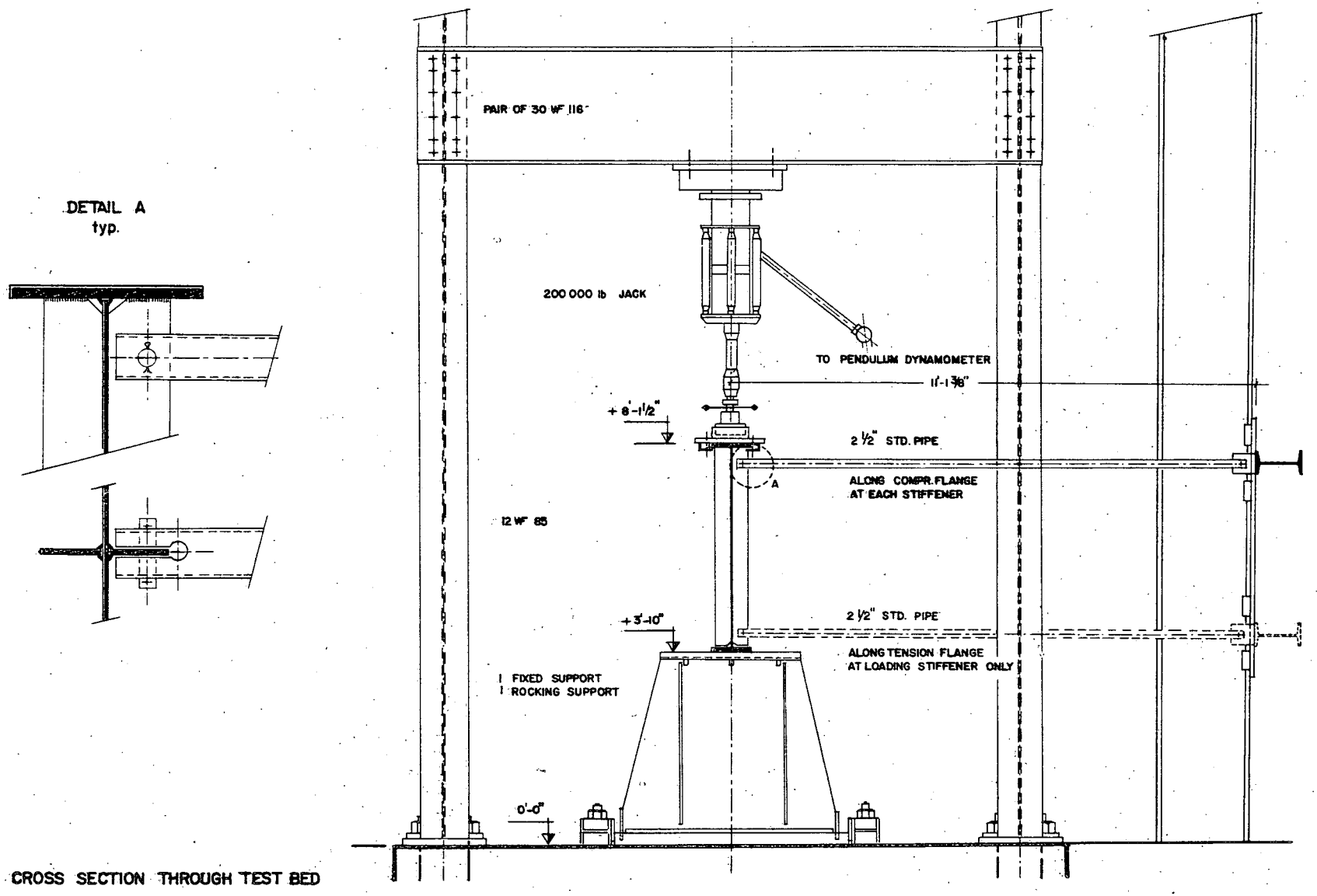

Fig. 2.4 - OVERALL VIEW OF TEST SETUP

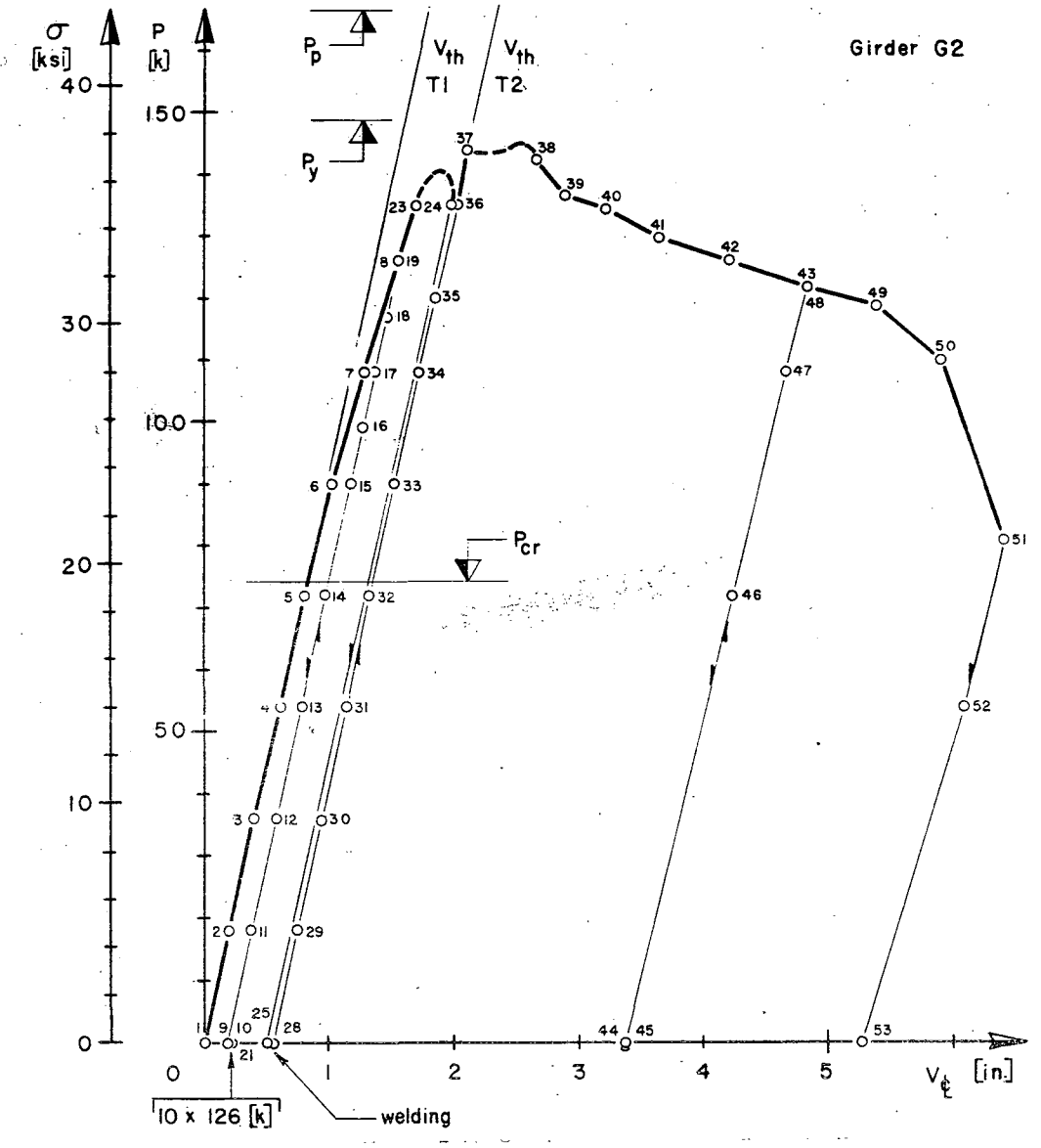

Fig. 2.5 Load-Deflection Curve of Girder G2

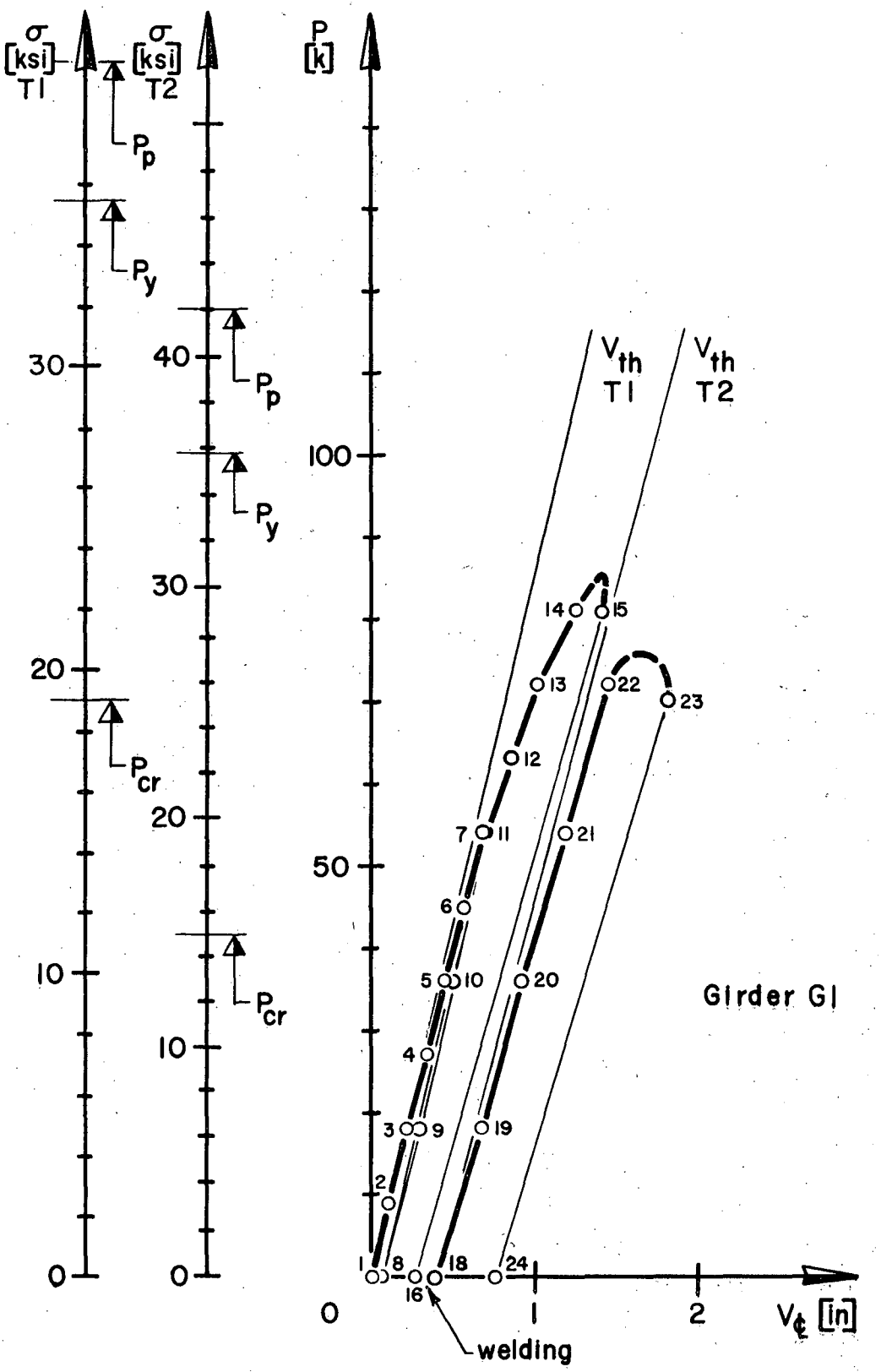

Fig. 2.6 Load-Deflection Curve of Girder G1

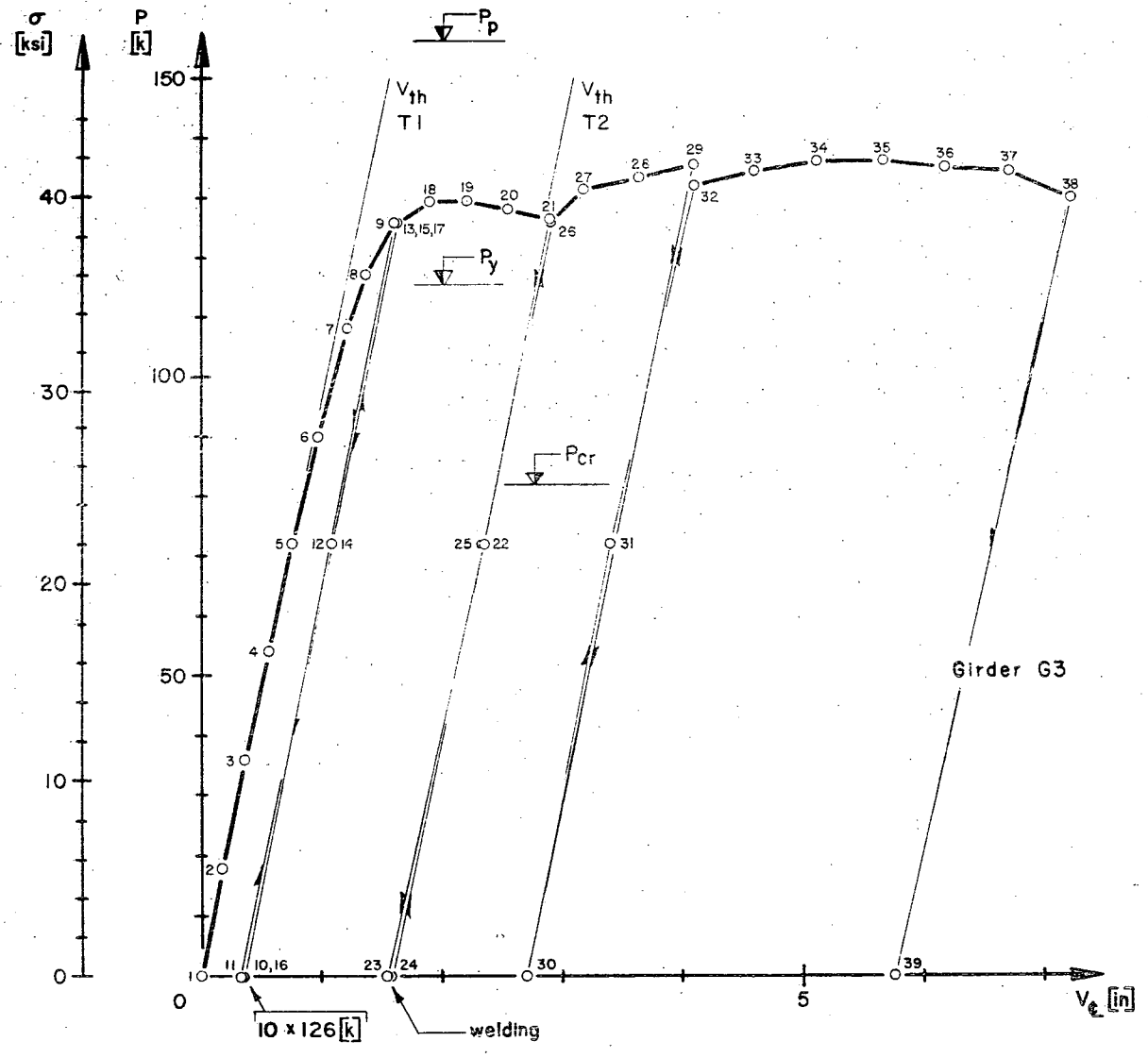

Fig. 2.7 Load-Deflection Curve of Girder G3

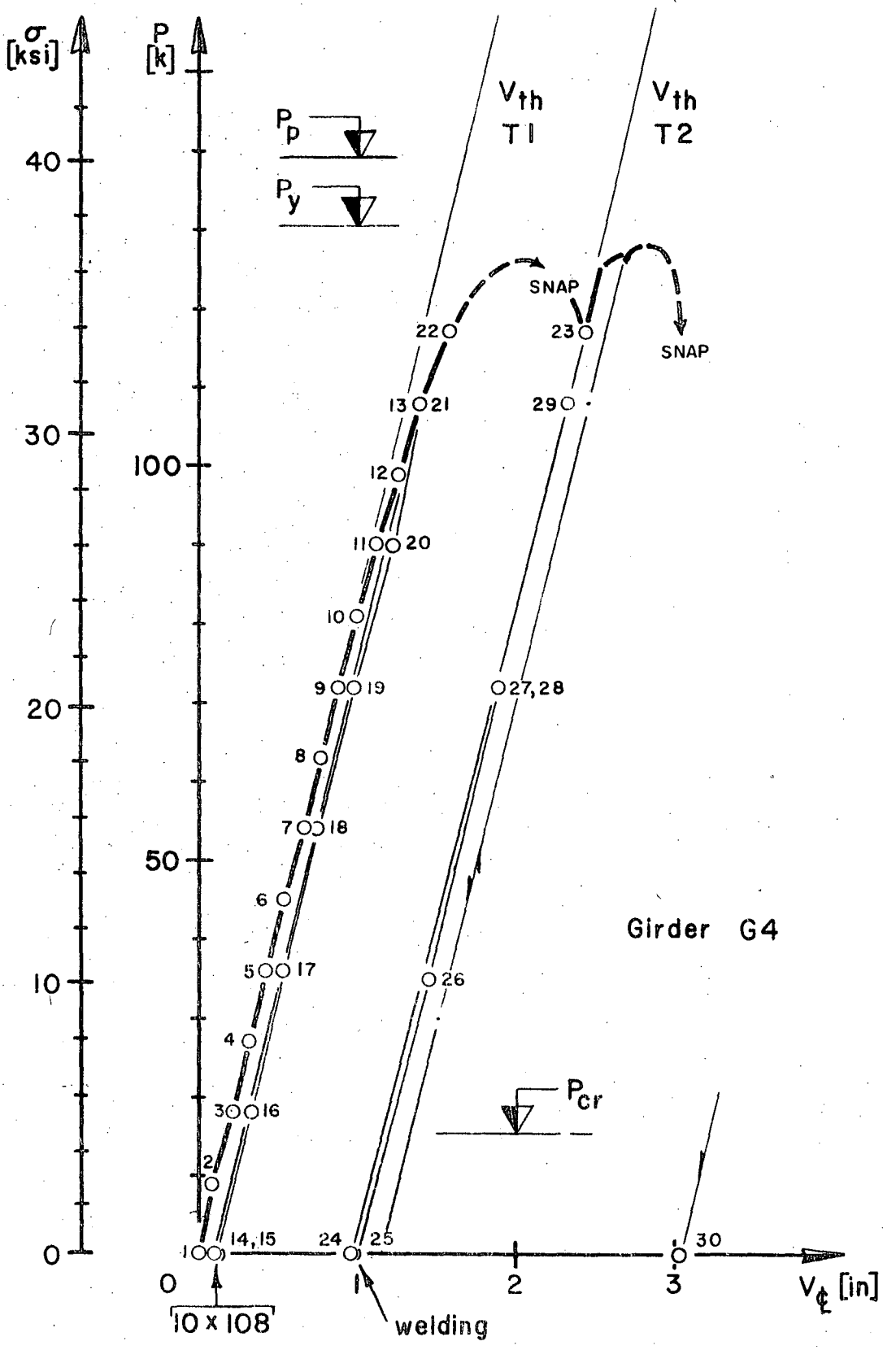

Fig. 2.8 Load-Deflection Curve of Girder G4

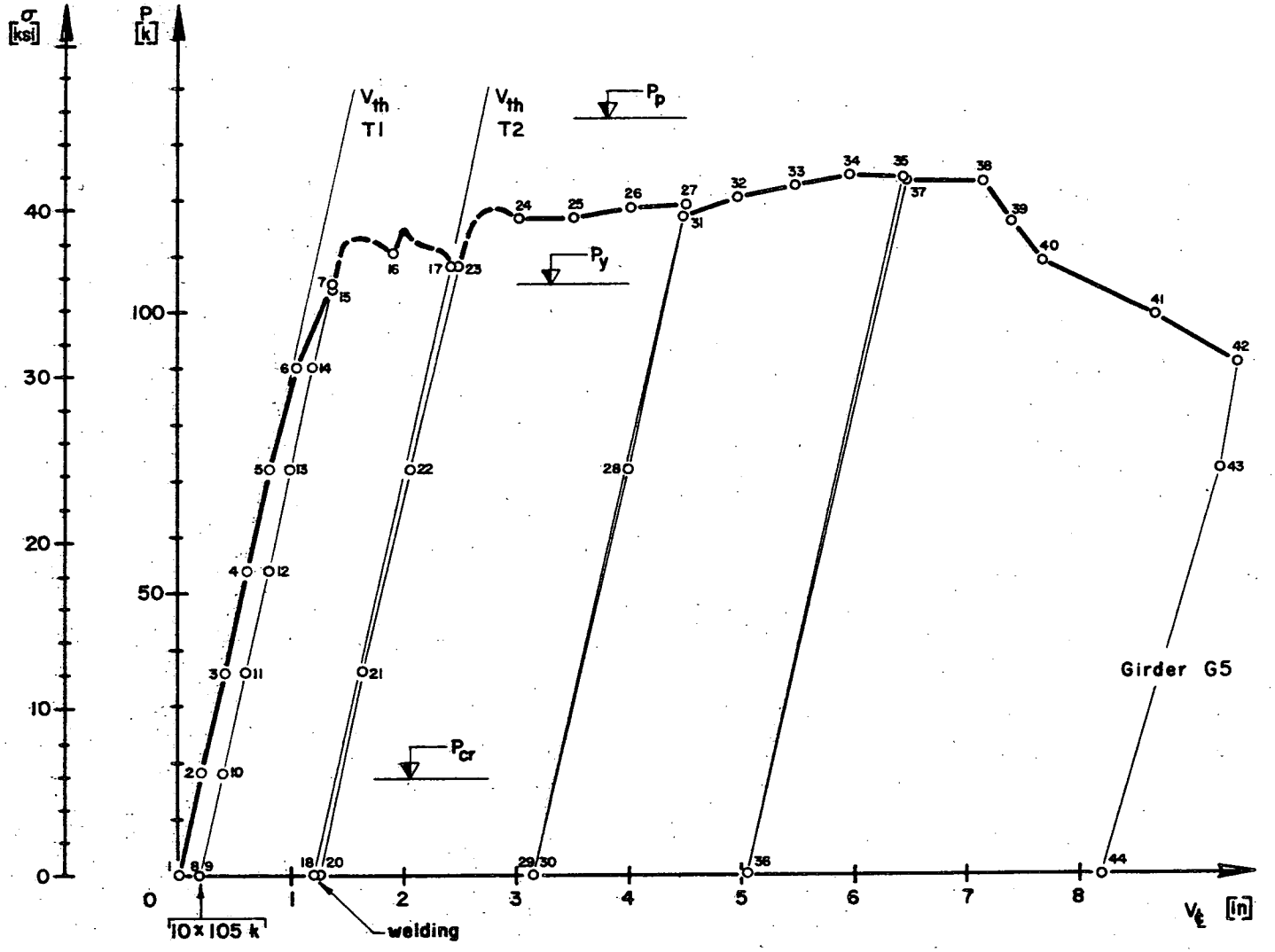

Fig. 2.9 Load-Deflection Curve of Girder G5

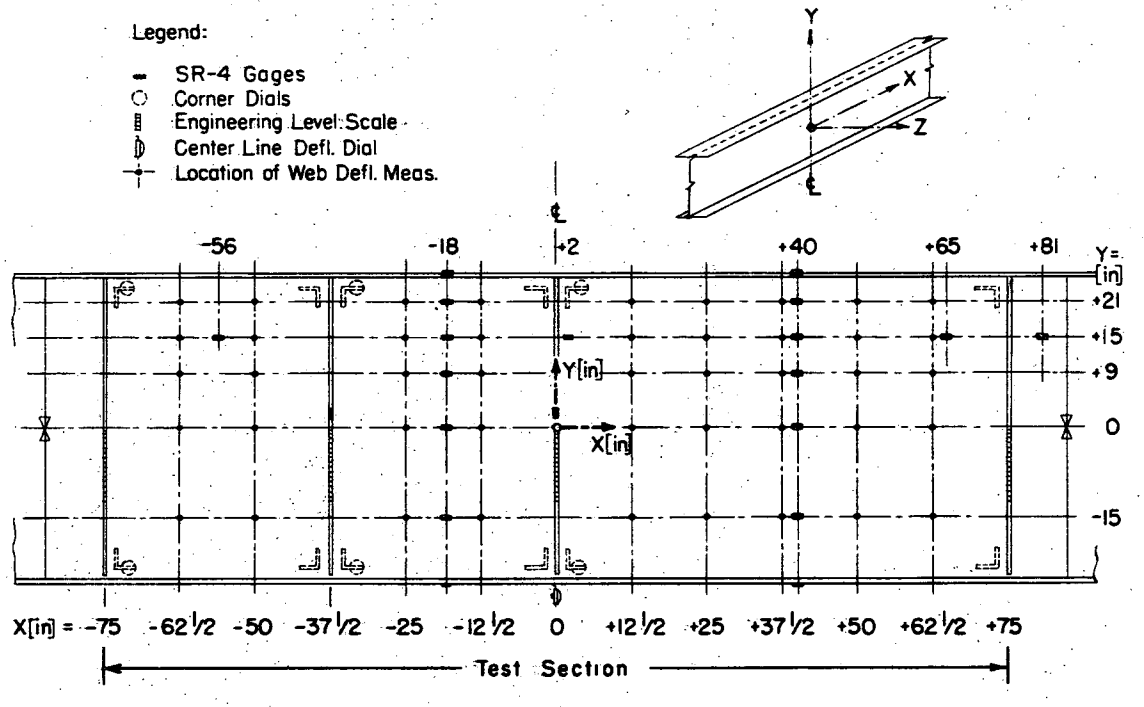

Fig. 2.10 Instrumentation

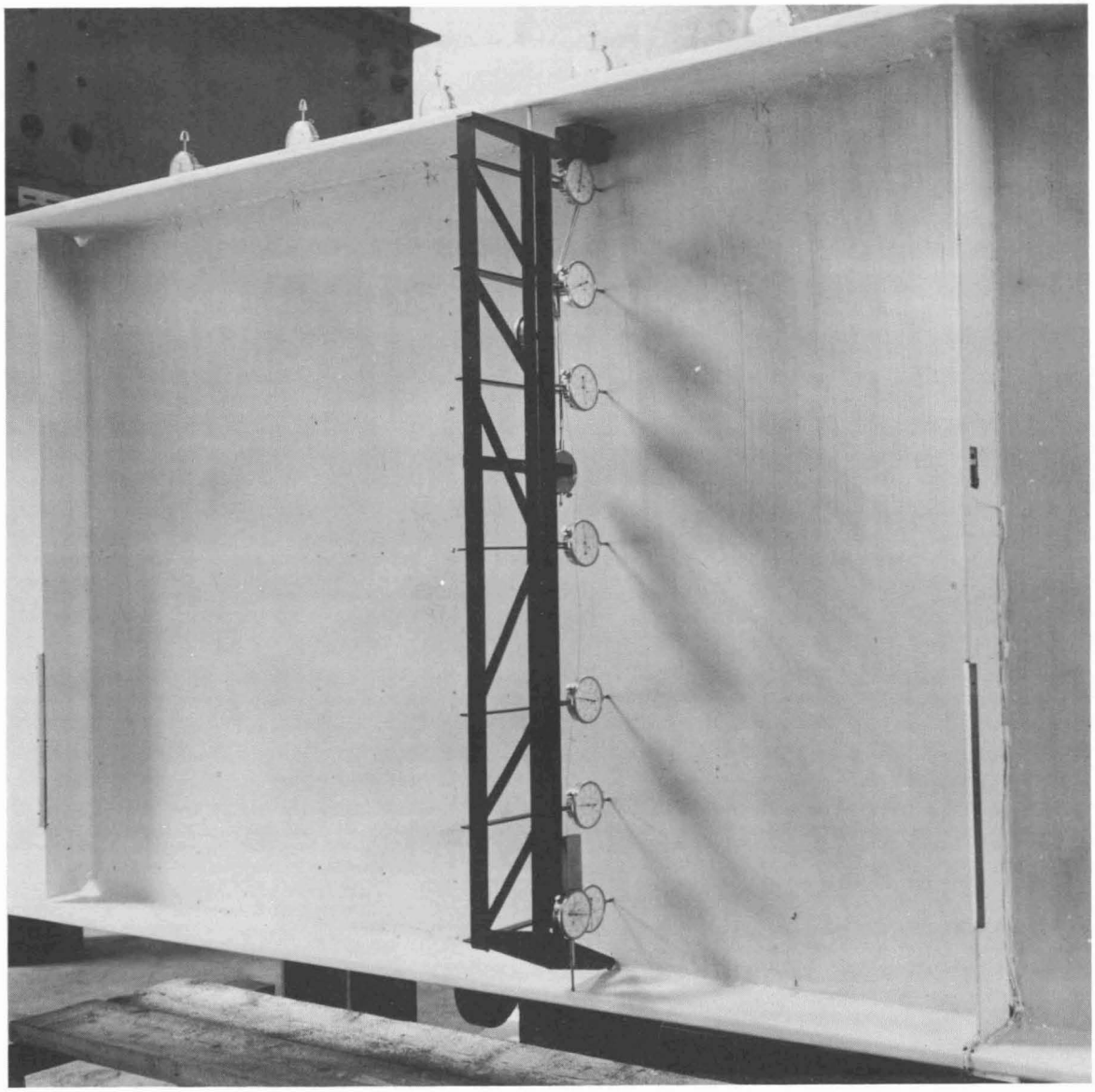

Fig. 2.11 Dial Rig for Web Deflection

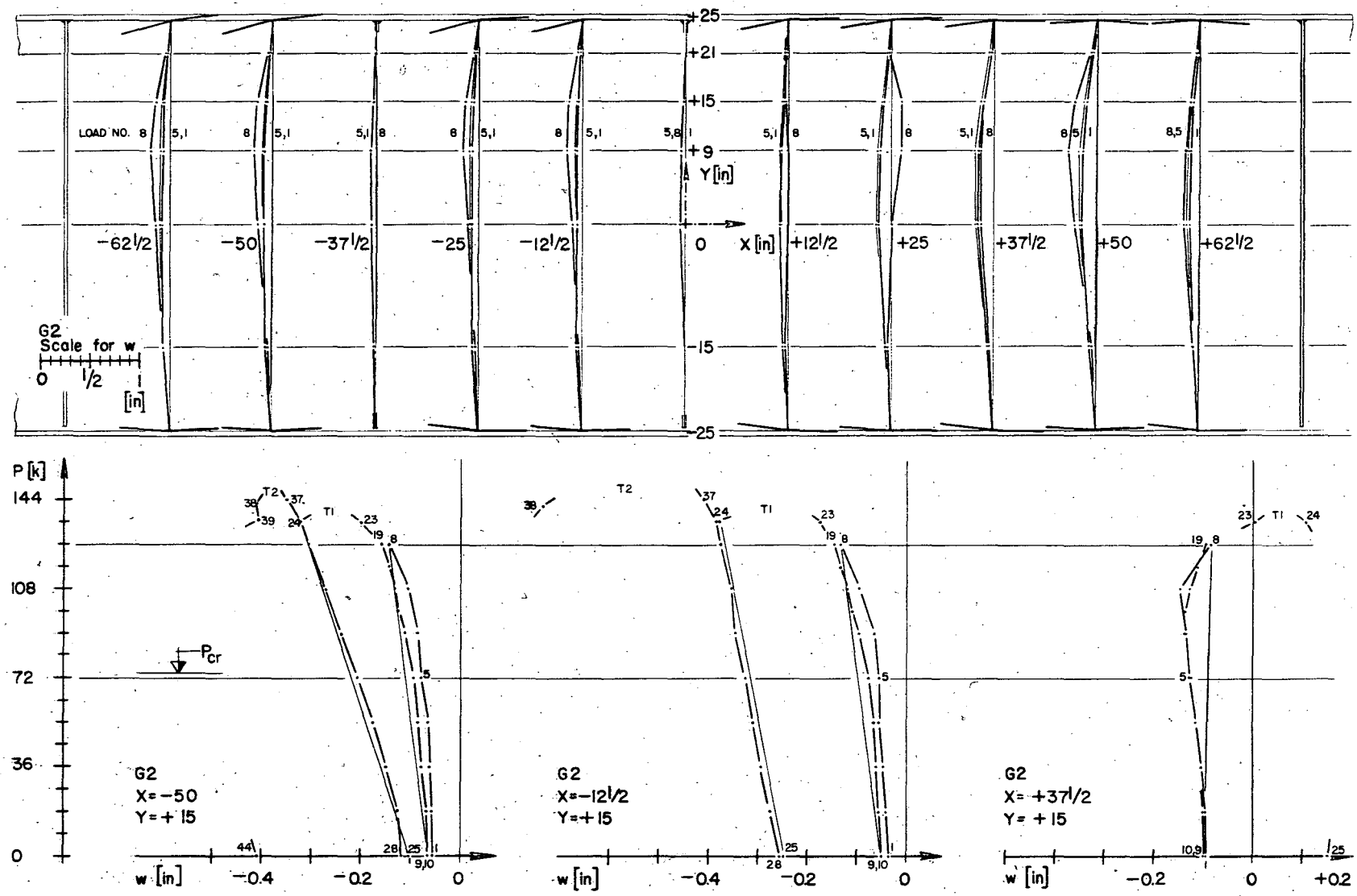

Fig. 2.12 Web Deflection of Girder G2

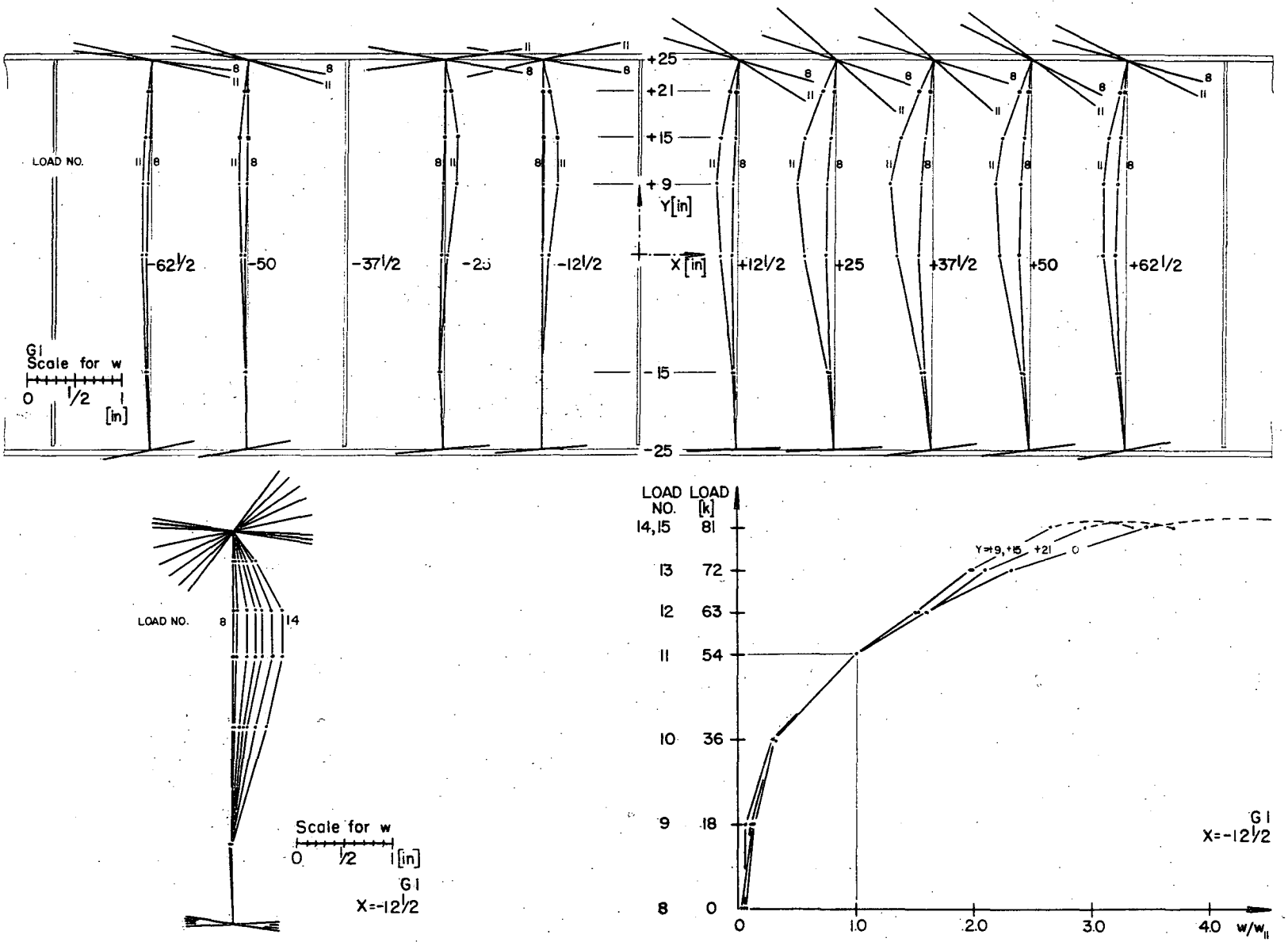

Fig. 2.13 Web Deflection of Girder G1

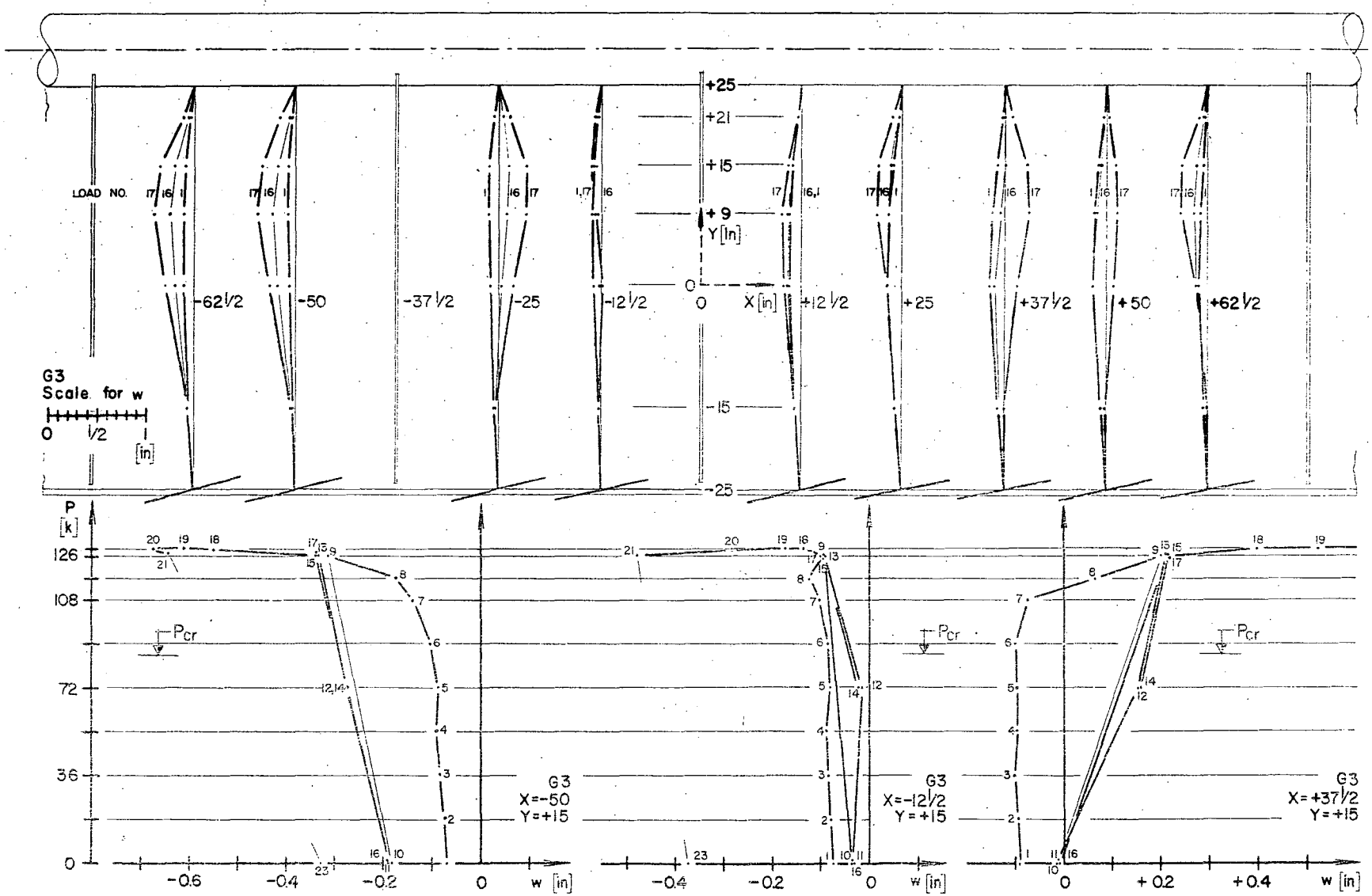

Fig. 2.14 Web Deflection of Girder G3

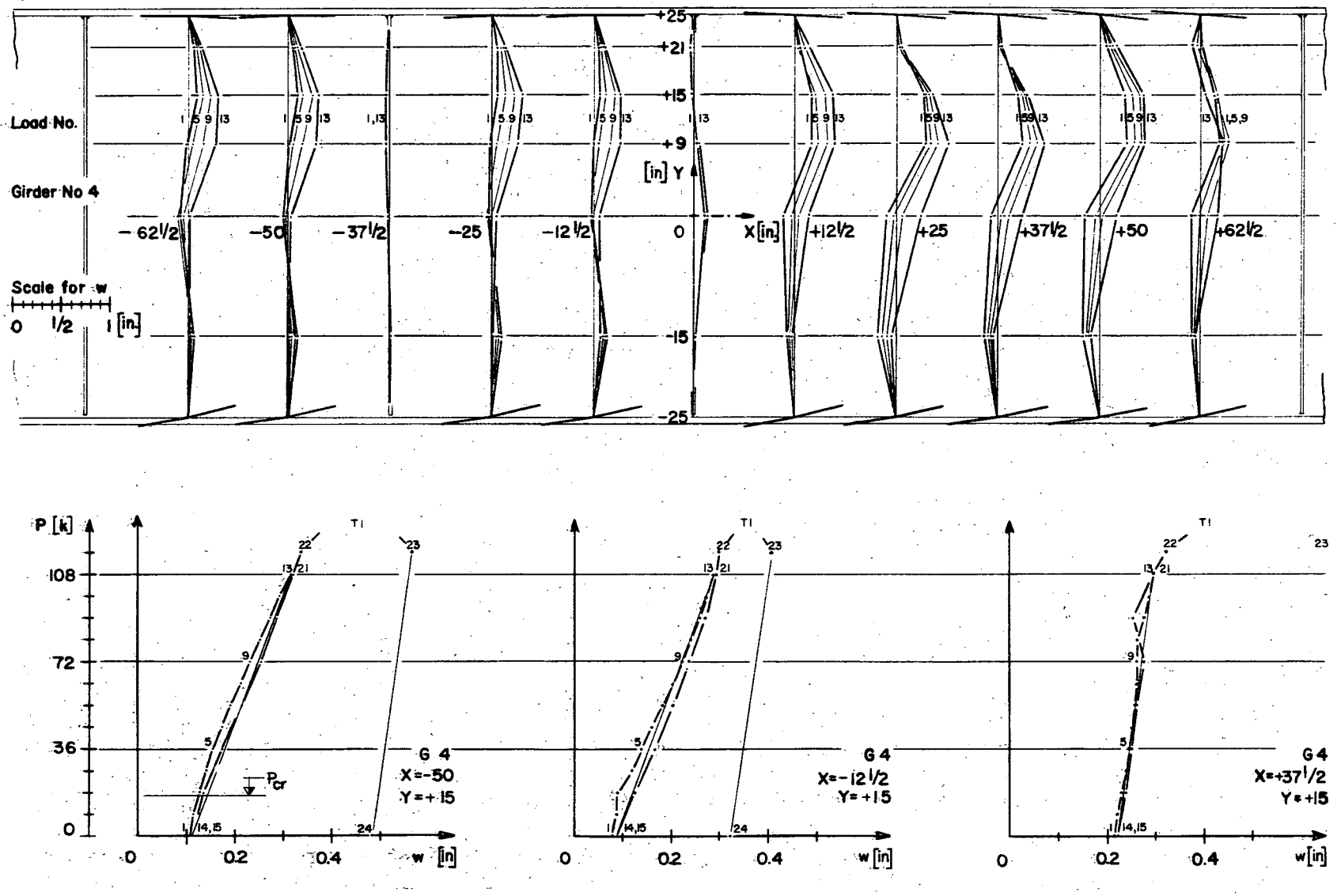

Fig. 2.15 Web Deflection of Girder G4

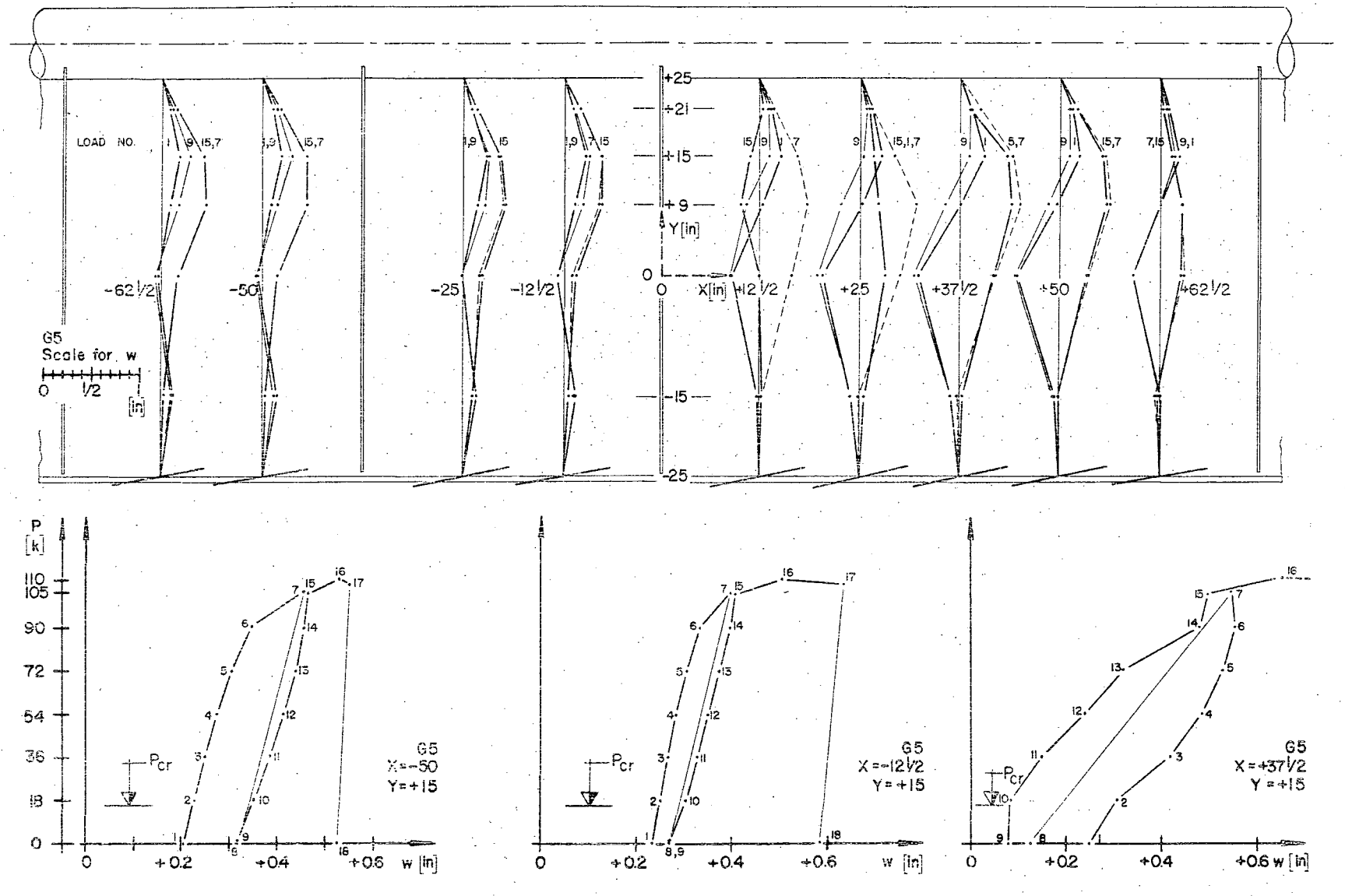

Fig. 2.16 Web Deflection of Girder G5

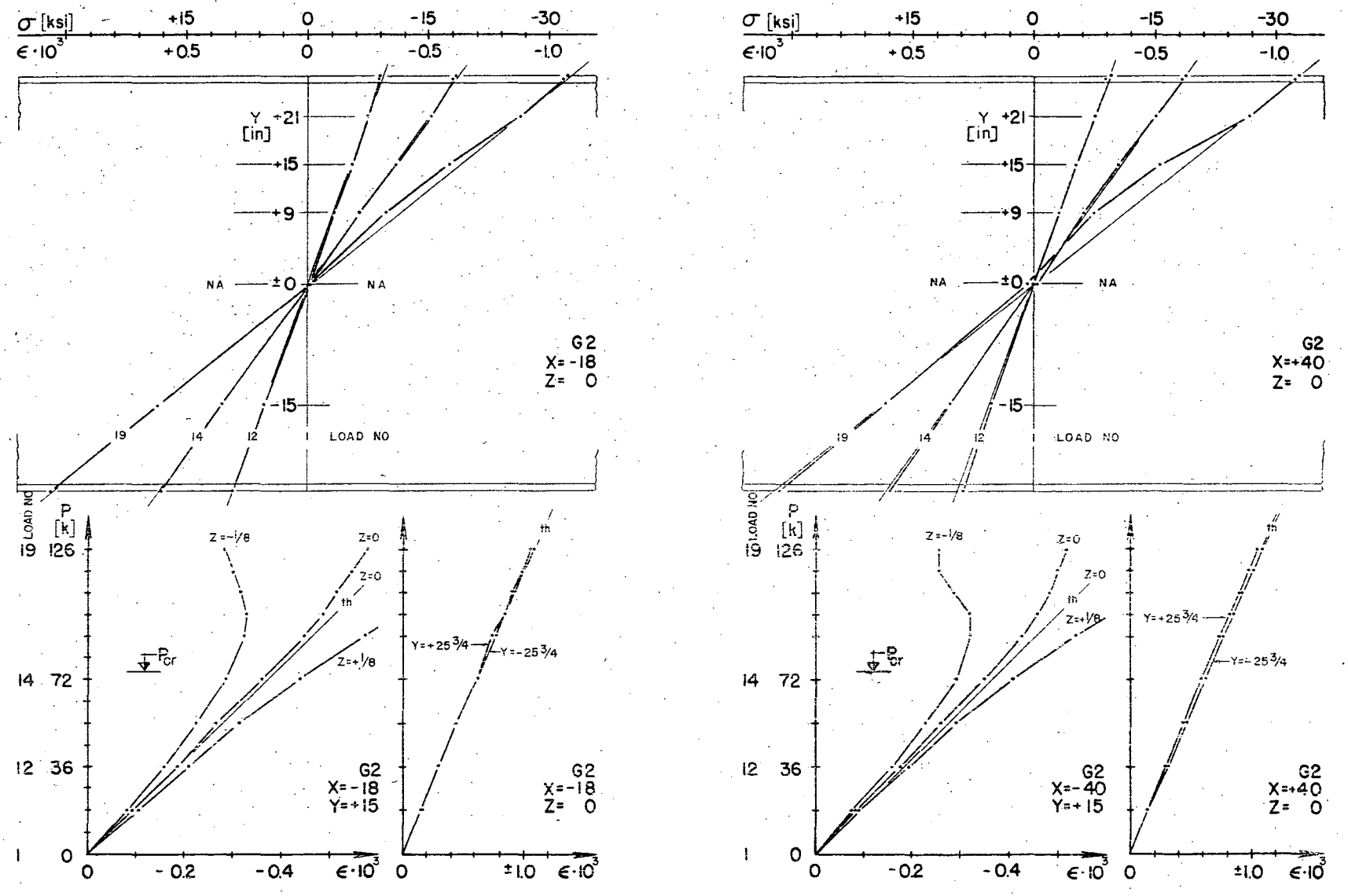

Fig. 2.17 Bending Strain in Girder G2

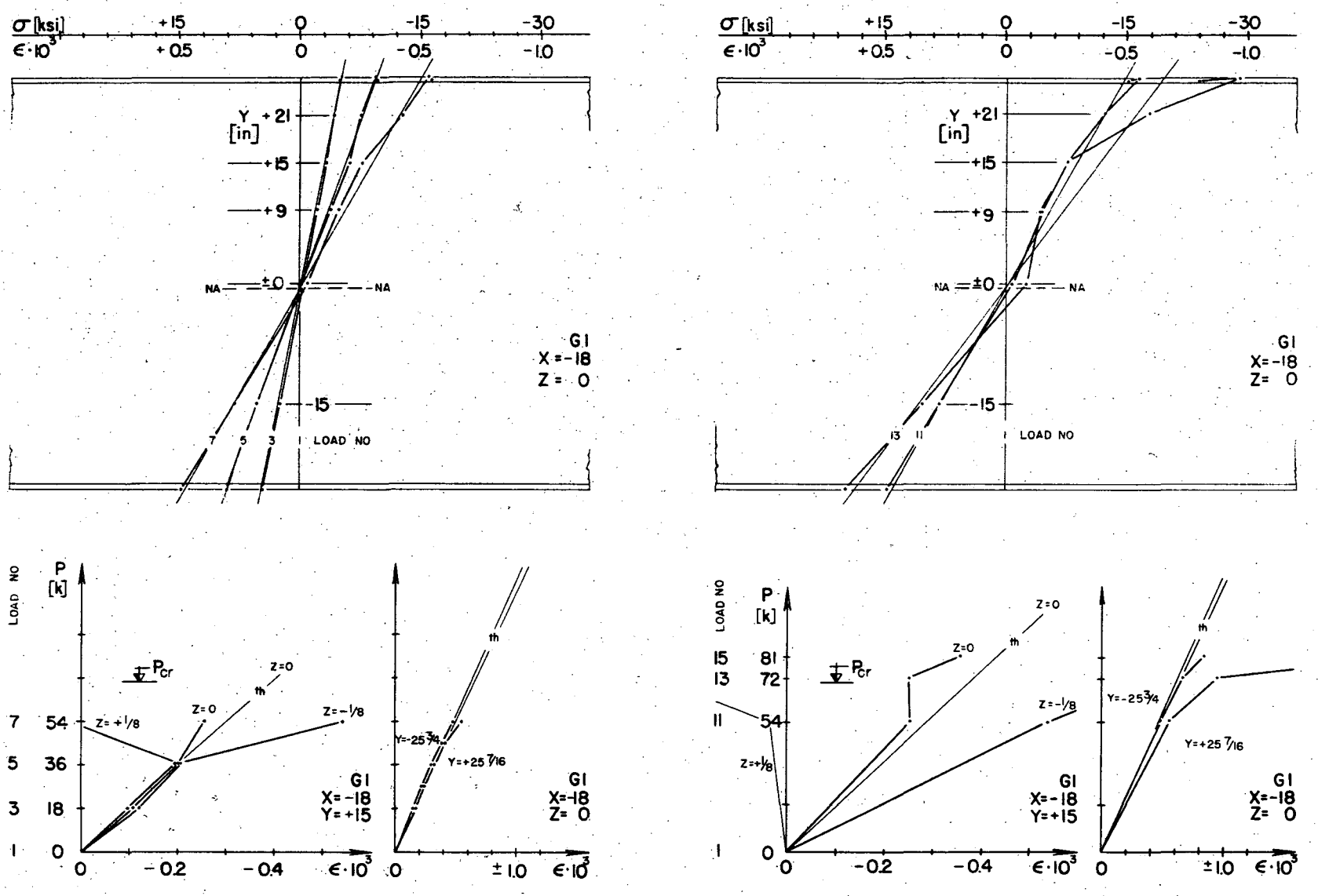

Fig. 2.18 Bending Strain in Girder G1

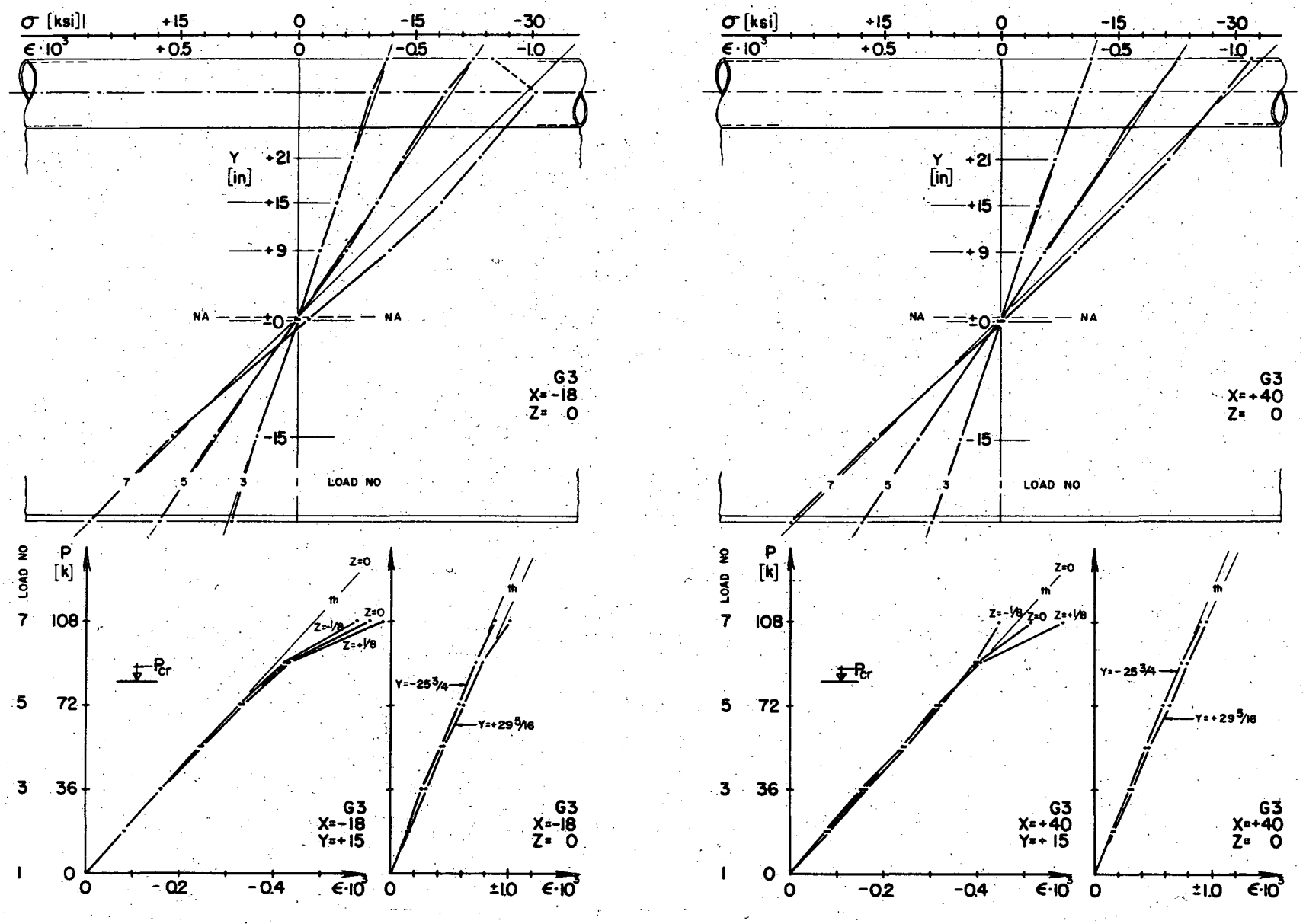

Fig. 2.19 Bending Strain in Girder G3

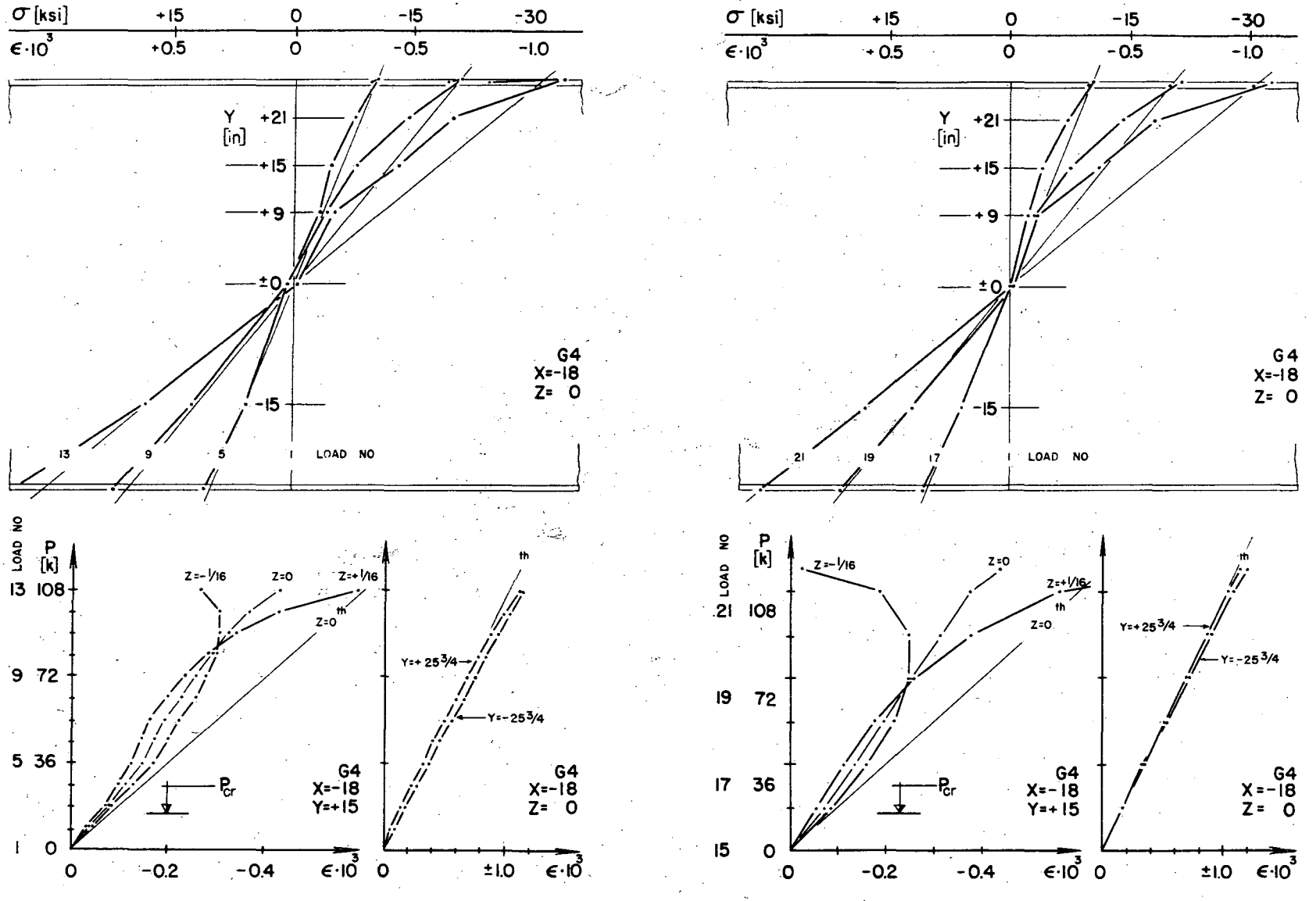

Fig. 2.20 Bending Strain in Girder G4

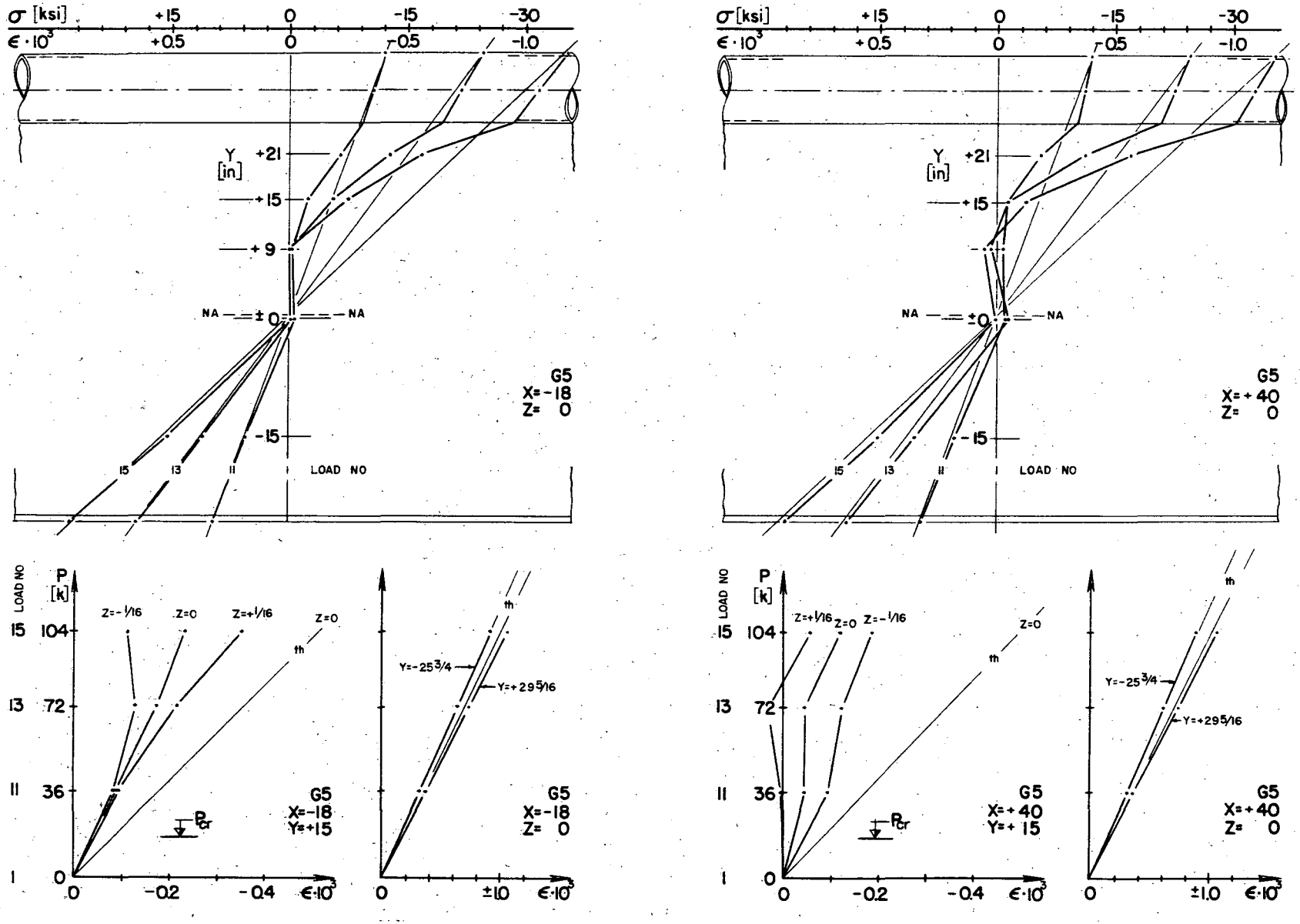

Fig. 2.21 Bending Strain in Girder G5

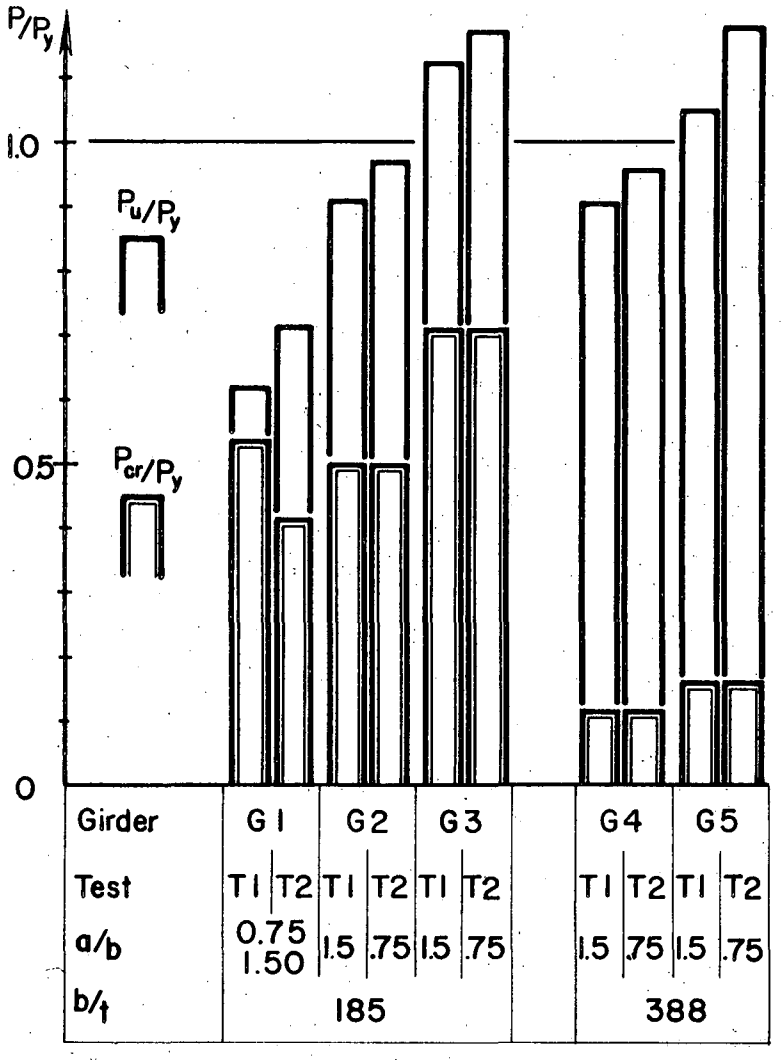

Fig. 2.22 - Graphical Summary of Loads, Non-Dimensionalized with P_y

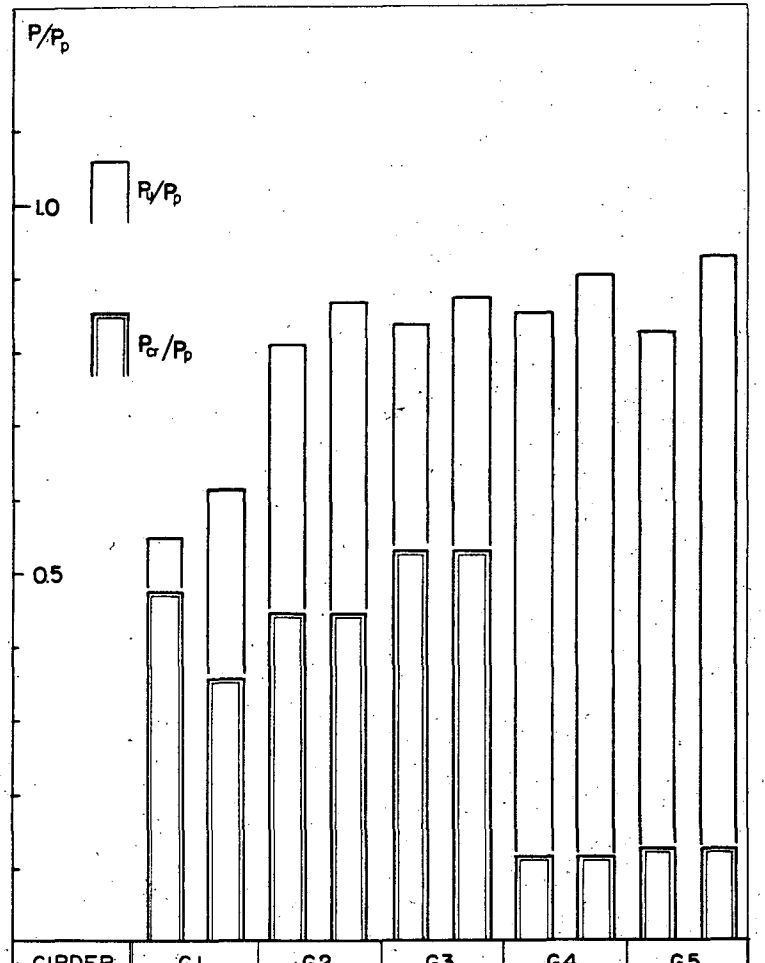

GIRDER	G1		G2		G3		G4		G5	
TEST	T1	T2	T1	T2	T1	T2	T1	T2	T1	T2
a/b	0.75&1.50		1.50	0.75	1.50	0.75	1.50	0.75	1.50	0.75
b/t	185						388			

Fig. 2.23 - Graphical Summary of Loads, Non-Dimensionalized with P_p

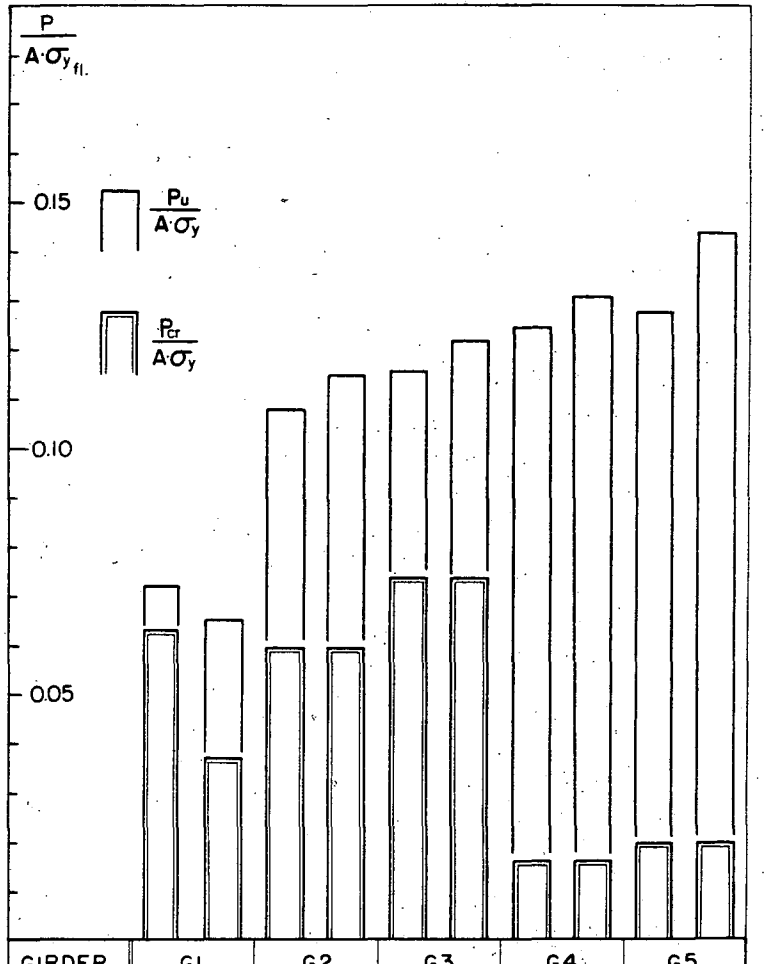

GIRDER	G1		G2		G3		G4		G5	
TEST	T1	T2	T1	T2	T1	T2	T1	T2	T1	T2
a/b	0.75&1.50		0.75	1.50	0.75	1.50	0.75	1.50	0.75	1.50
b/t	185						388			

Fig. 2.24 - Graphical Summary of Loads, Non-Dimensionalized with $A\sigma_y$

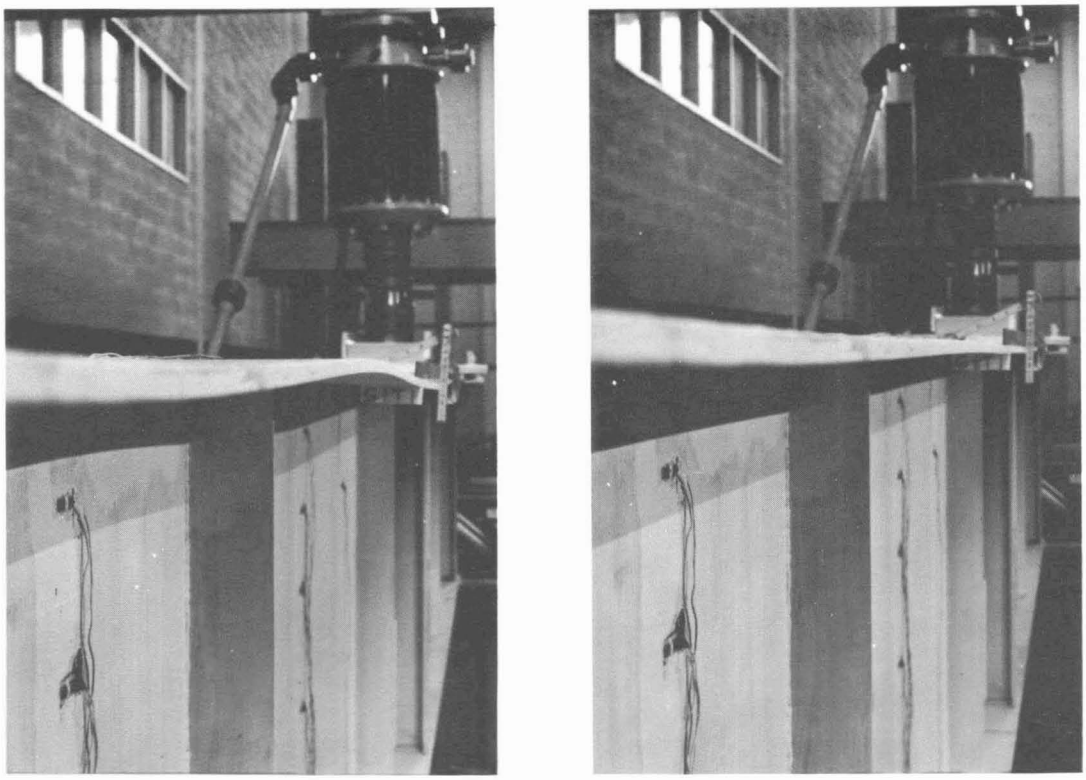

Fig. 2.25 Flange Deflections in Girder G-1 (Load No. 7 and 8)

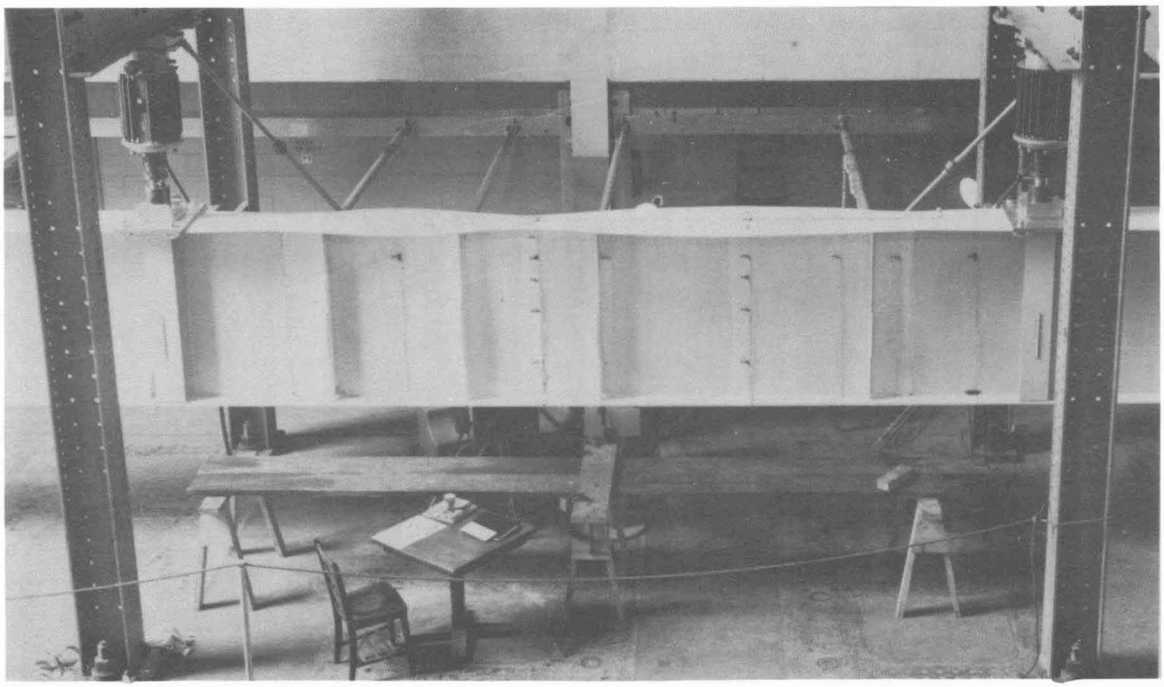

Fig. 2.26 Girder G1 at Ultimate Load

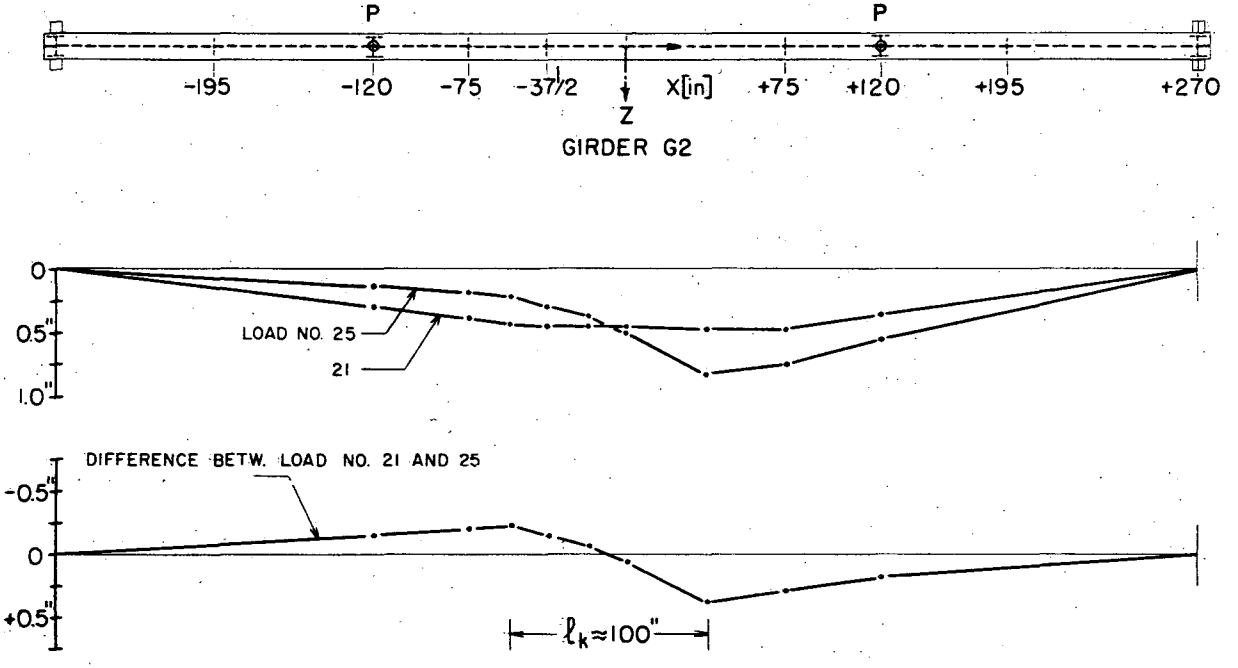

Fig. 2.27 Lateral Deflection of Compression Flange, G2-T1

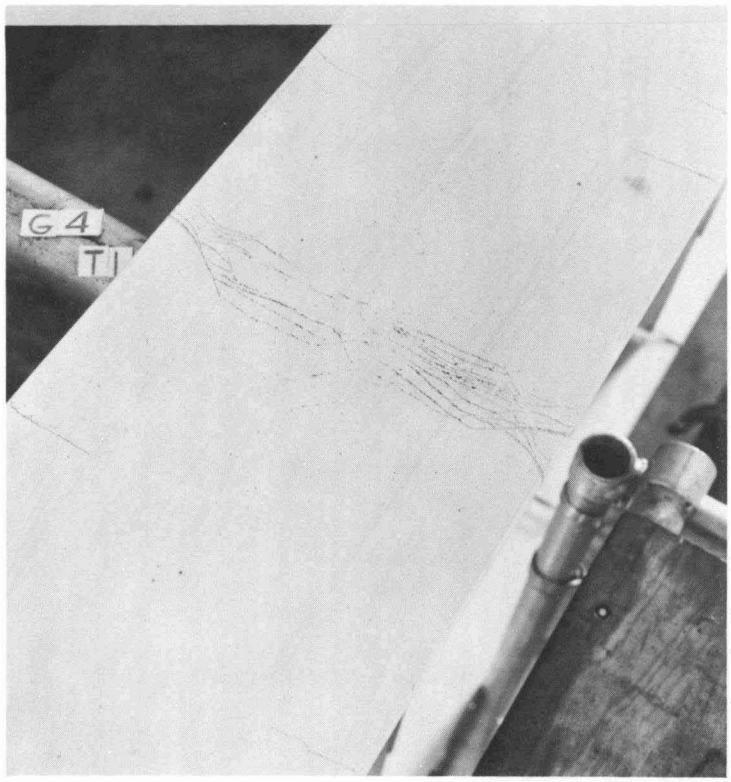

Fig. 2.28 Typical Yield Line Pattern in Compression Flange

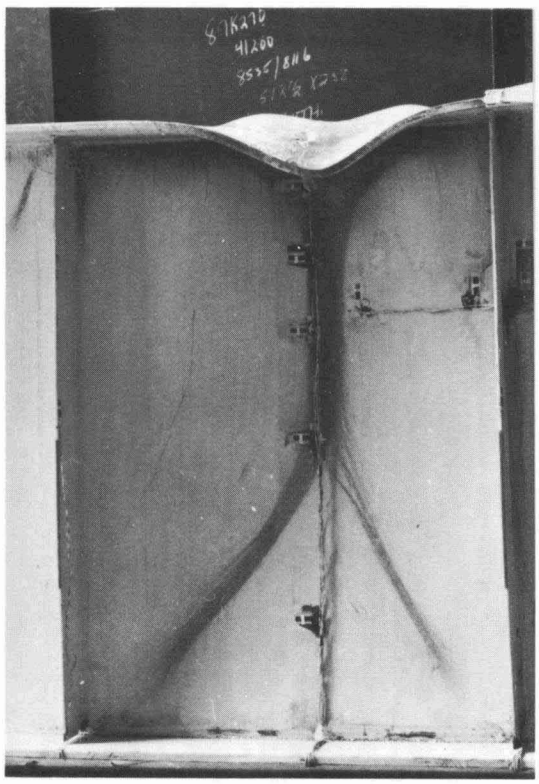

Fig. 2.29 Local Torsional Buckling of Compression Flange (G2, T2)

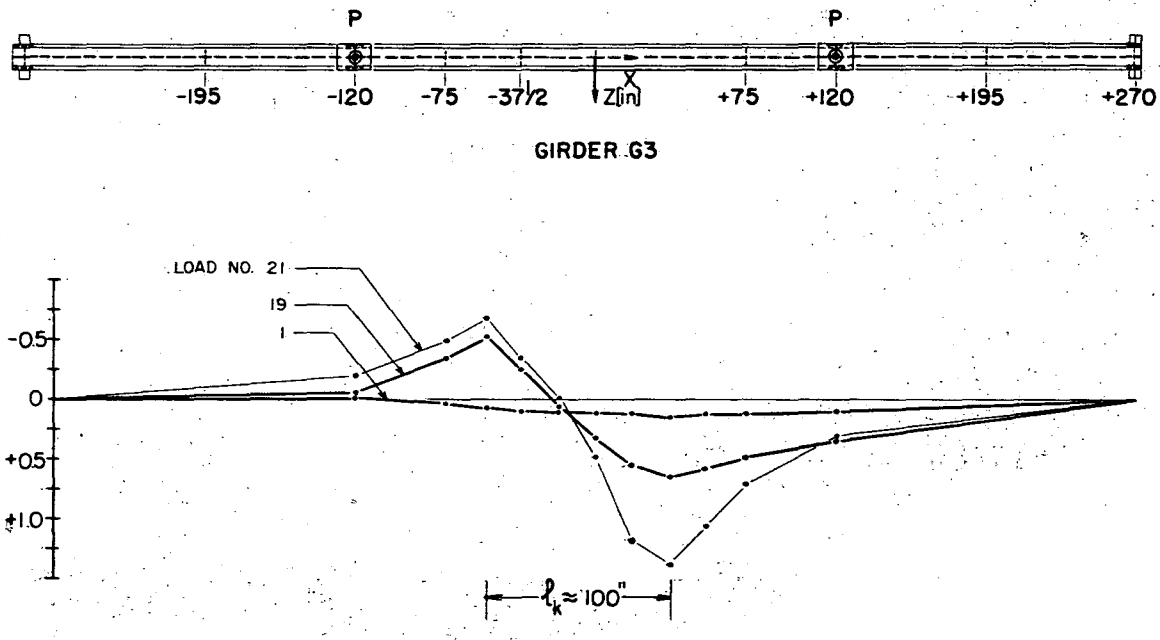

Fig. 2.30 Lateral Deflection of Compression Flange, G3-T1

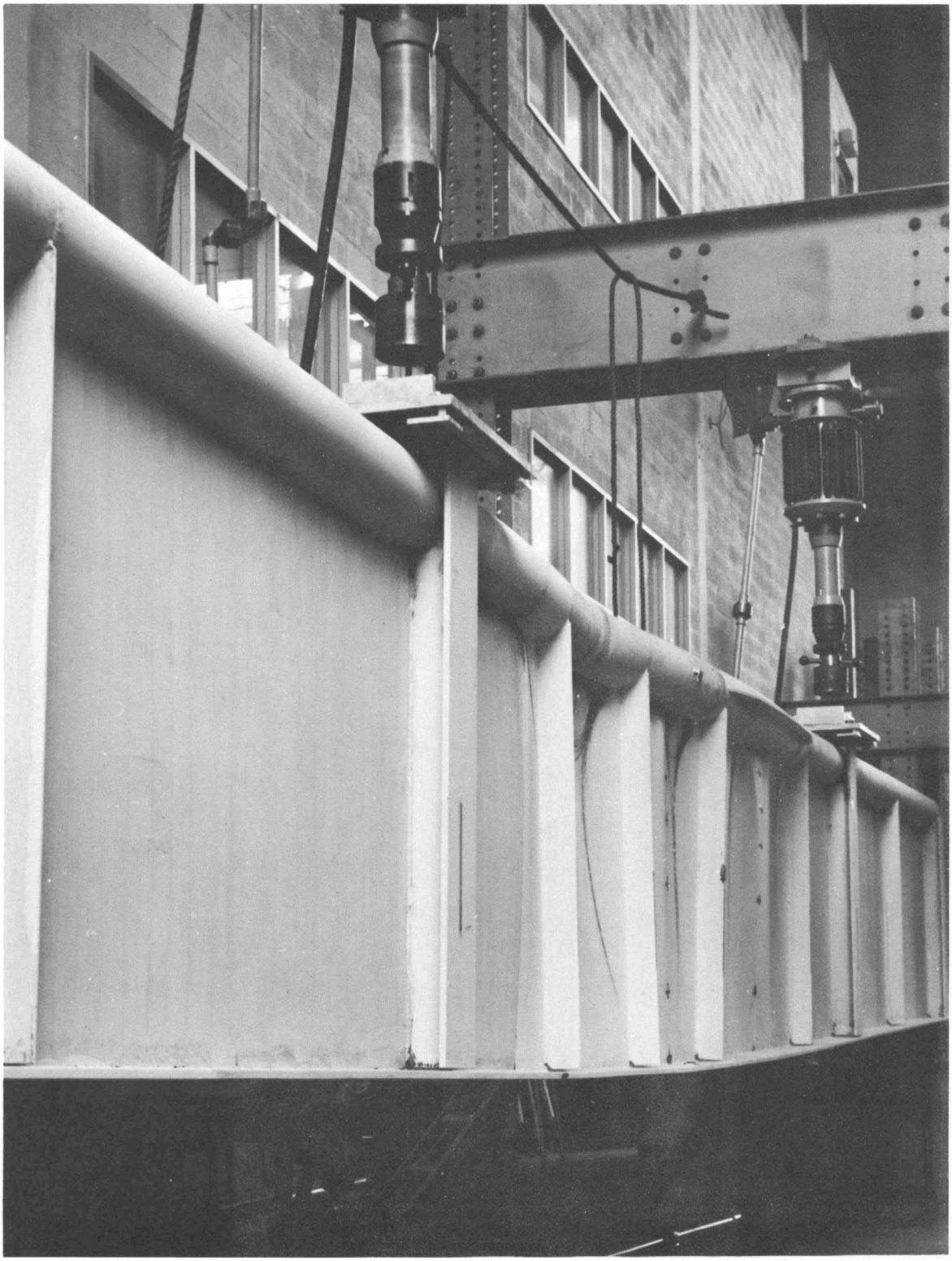

Fig. 2.31 Girder G3 after Testing

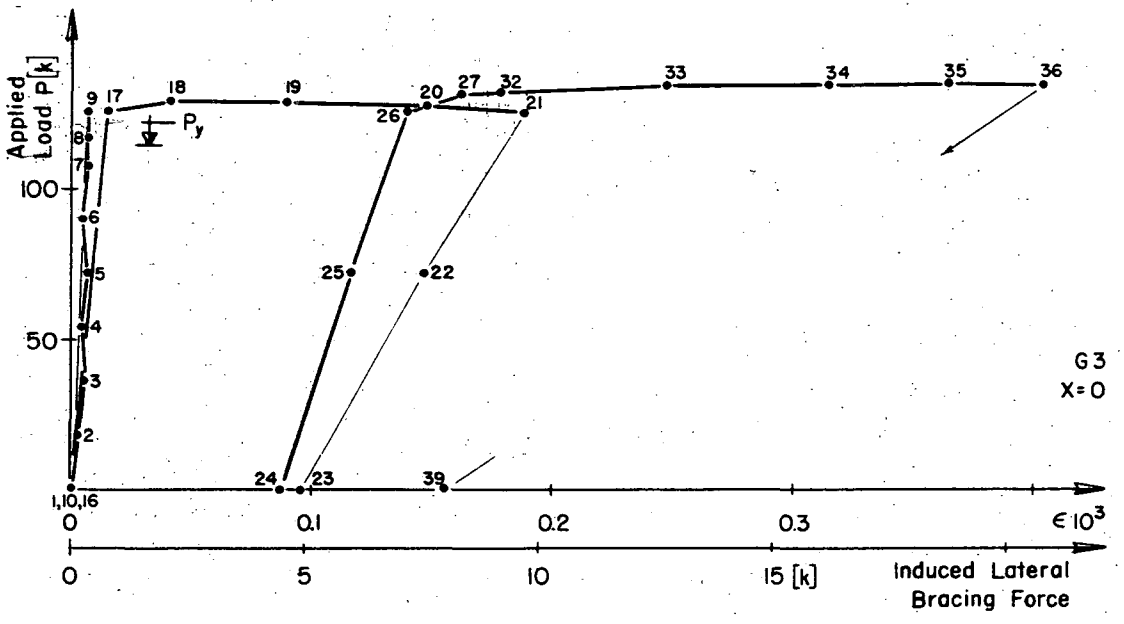

Fig. 2.32 Induced Lateral Bracing Force

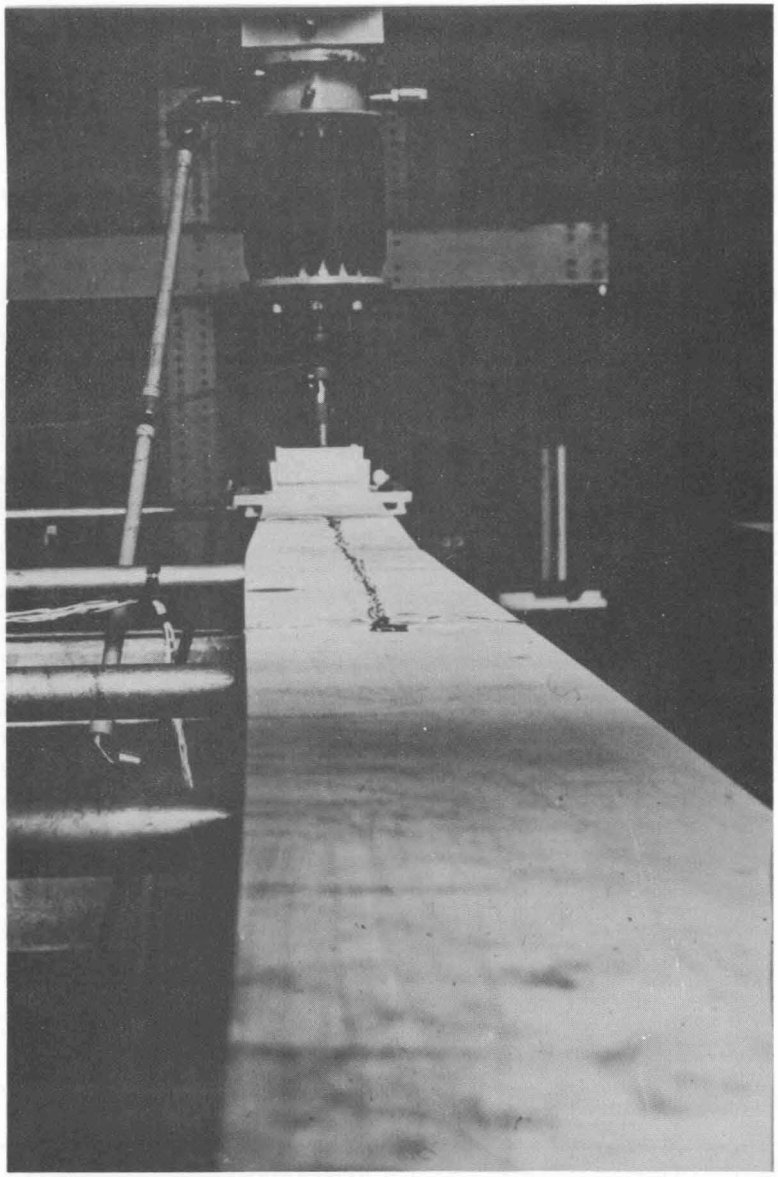

Fig. 2.33 Lateral Buckling of the Compression Flange (G4, T1)

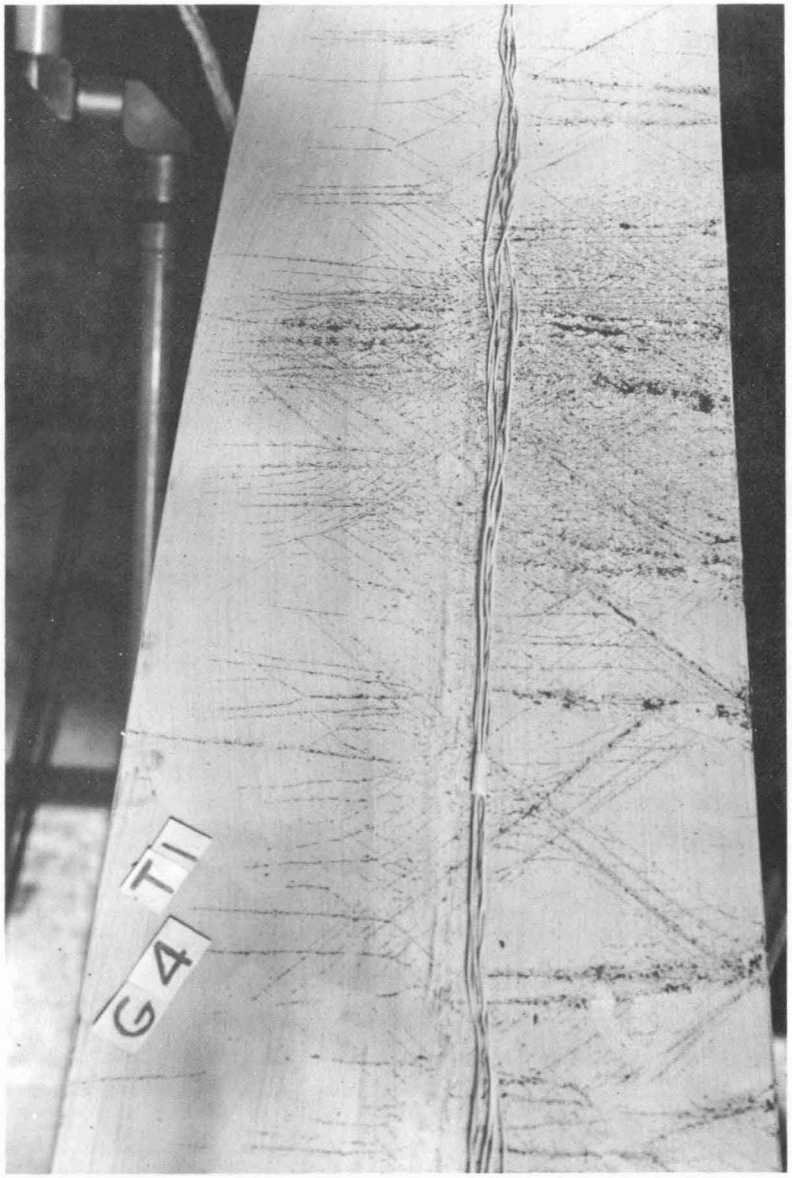

Fig. 2.34 Yield Lines in the Compression Flange (G4, T1)

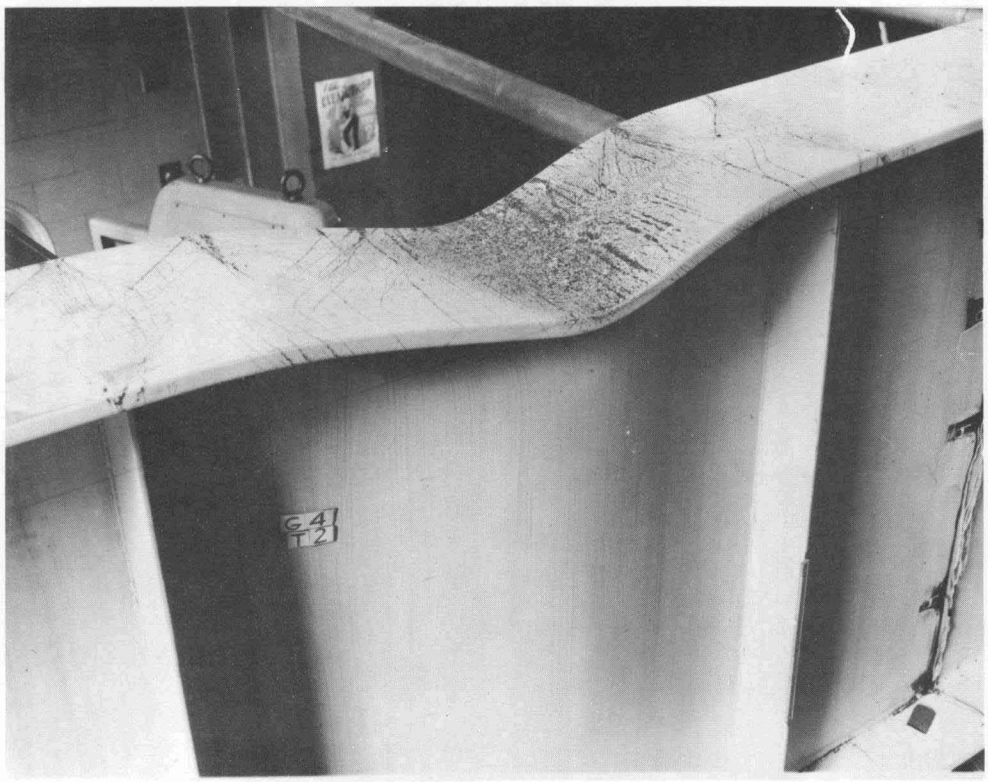

Fig. 2.35 Vertical Buckling of the Compression Flange (G4, T2)

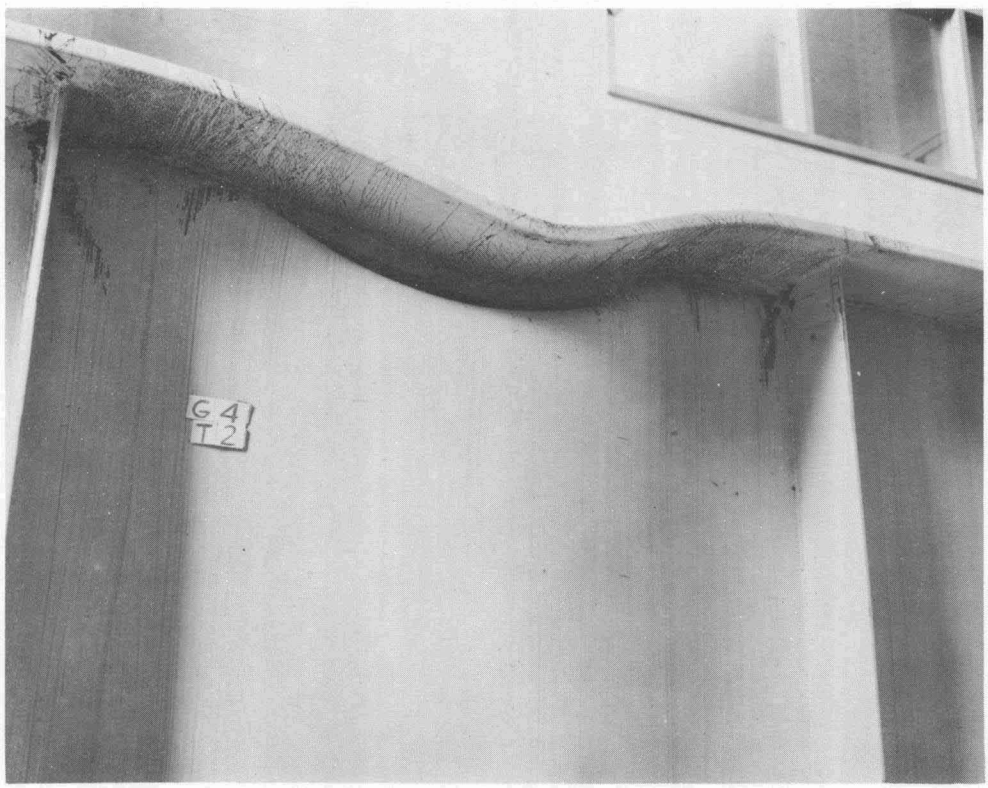

Fig. 2.36 Vertical Buckling of the Compression Flange (G4, T2)

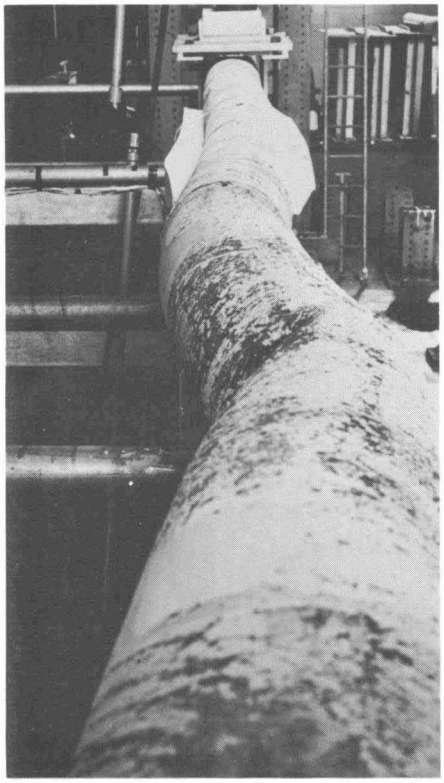

Fig. 2.37 Top Flange of Girder G5 after Testing

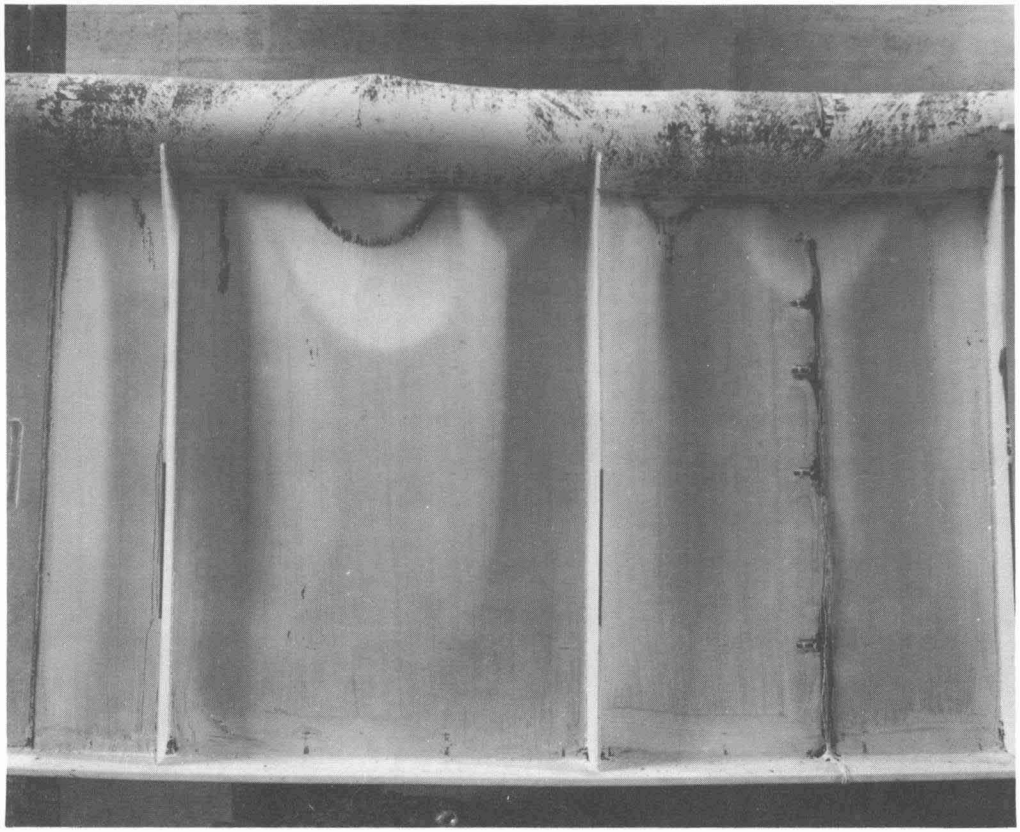

Fig. 2.38 Failure of Girder G5, Test T2

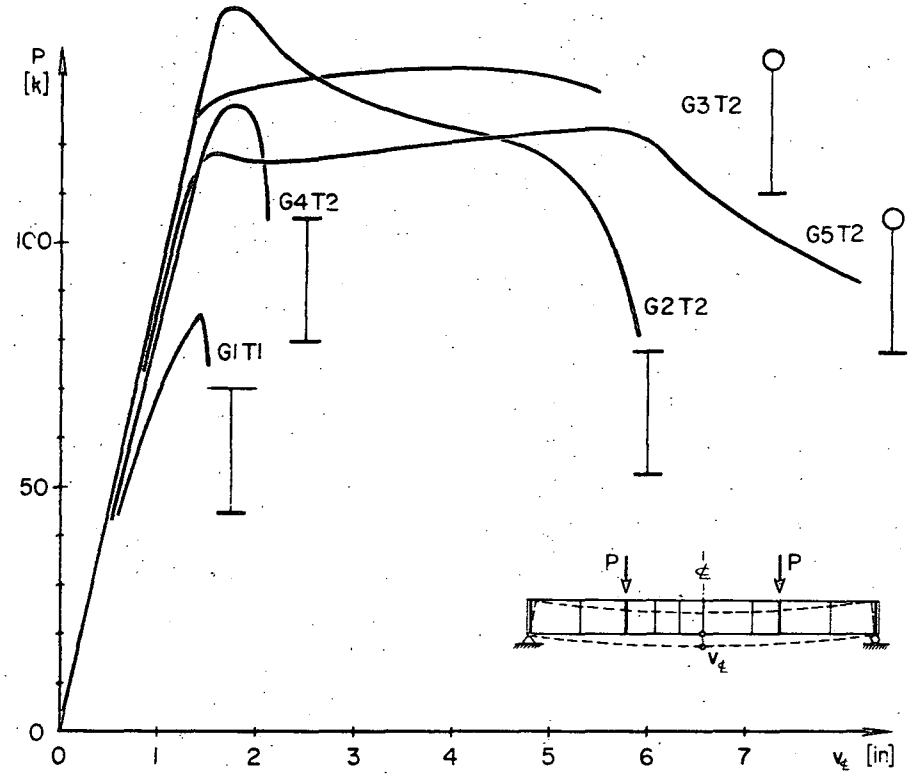

Fig. 2.39 Comparision of Load-Deflection Curves

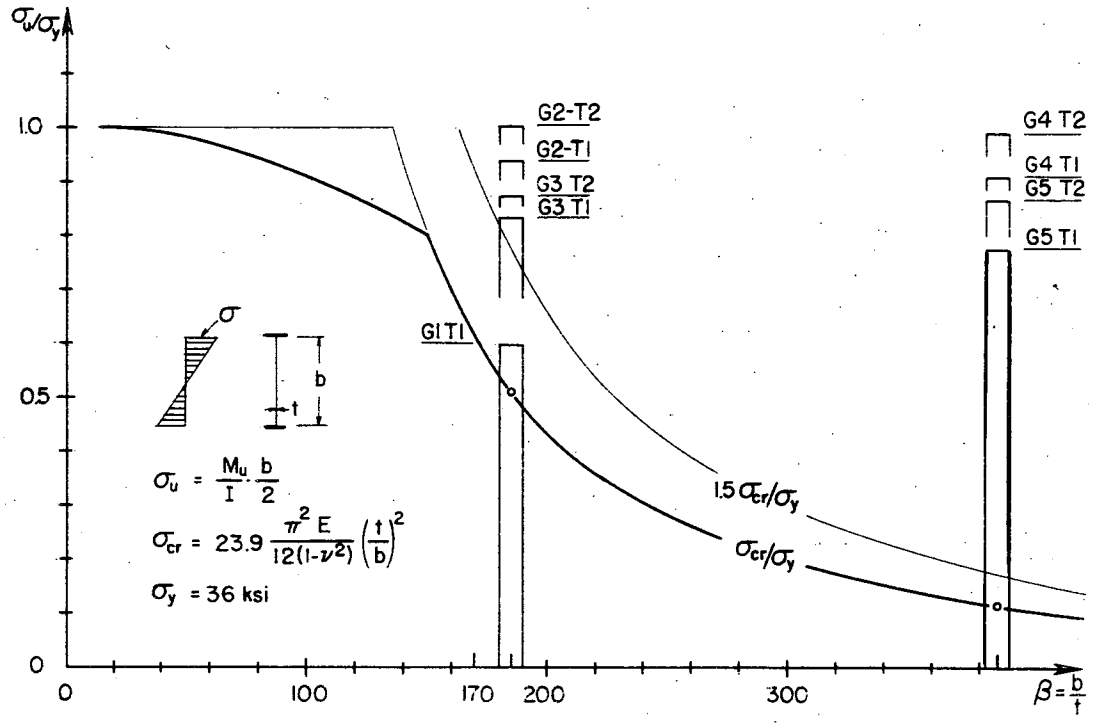

Fig. 2.40 Post-Buckling Strength